A POWERED SELF-CONTAINED KNEE AND ANKLE PROSTHESIS FOR NEAR NORMAL GAIT IN TRANSFEMORAL AMPUTEES

By

Frank Charles Sup IV

Dissertation

Submitted to the Faculty of the

Graduate School of Vanderbilt University

in partial fulfillment of the requirements

for the degree of

DOCTOR OF PHILOSOPHY

in

Mechanical Engineering

August, 2009

Nashville, Tennessee

Approved:

Dr. Michael Goldfarb

Dr. George E. Cook

Dr. Nilanjan Sarkar

Dr. Eric J. Barth

Dr. Robert J. Webster III

To my wife and son

ACKNOWLEDGMENTS

Reflecting upon my graduate career, I am deeply grateful to the many people whose help, insight, and guidance has brought me to where I am at today. I would first like to thank Dr. Ty Newell, who helped a former student find his direction and motivated him to enter graduate school. Next, I would like to thank my advisor Dr. Michael Goldfarb for taking me on as a student and sharing his knowledge and insight over the duration of my graduate career. He has taught me to think creatively and independently and has given me an invaluable tool set to tackle complex problems. I would also like to express my appreciation to the members of my dissertation committee, Dr. George Cook, Dr. Nilanjan Sarkar, Dr. Eric Barth and Dr. Robert Webster, for their time and support. I thank the National Institutes of Health, grant R01EB005684-01, for funding this work.

The sum is greater than the parts. This has certainly proven to be true of my collaboration on this work with the soon to be Dr. Atakan Varol. His rigor and genius helped keep the project on track and above expectations. I look forward to seeing the fruition of his work beyond graduation. All the members of the Center for Intelligent Mechatronics during my time here have been integral and deserve special recognition. The lab fosters a collaborative environment that allows all of the members to push beyond their bounds. I thank Dr. Thomas Withrow and Jason Mitchell who have been invaluable for their advice and assistance. A special thanks goes to Craig who went above and beyond in helping us test and who without the project could not have gone so far.

It almost goes without saying that I am incredibly grateful to my entire family for their unfailing love, support, confidence and encouragement. I would especially like to thank my parents for everything they

have done for me over the years. I thank them for pushing me to excel, for teaching me to love learning and for encouraging me to be a better person. Most importantly, I would like to acknowledge the incredible tolerance and patience displayed by my wife, Lara, during my graduate career. It has not been easy, but she has made it fun. Her continuous love, support and sacrifice has helped make this dream a reality. She helps me to find the best in myself and I look forward to taking on the next challenge with her by my side. Finally, I thank my son, Frank, for keeping me smiling and still loving his Daddy who sometimes had to work late.

TABLE OF CONTENTS

Page

LIST OF FIGURES

Page

LIST OF TABLES

Page

CHAPTER I

Overview

Introduction and Motivation

There are more than 300,000 transfemoral amputees in the United States [1] (i.e., an incidence of approximately one per thousand people), with 30,000 new transfemoral amputations conducted each year [2]. If similar trends hold across the world population, one would expect approximately 7 million transfemoral amputees worldwide. The lower limb amputee is faced with an extraordinary loss in power and mobility post amputation. Perhaps the most significant limitation of existing prosthetic technologies is the inability to provide net power at the joints. The loss of net power generation at the lower limb impairs the ability of the prosthesis to restore biomechanically normal locomotive function during many locomotive activities, including level walking, walking up stairs and slopes, running and jumping [3-10]. In the absence of net power generation at the knee and ankle, transfemoral amputees with passive prostheses have been shown to expend up to 60% more metabolic energy [11] and exert three times the affected-side hip power and torque [9] when compared to healthy subjects during level walking.

The current generation of state-of-the-art prosthetic knee joints are microprocessor controlled dampers, such as the Otto Bock C-Leg, Ossur Rheo Knee, and the Freedom Innovations Plié knee, Fig. 1-1. These knee joints control either hydraulic or magnetic rheological fluid for the modulation of the damping in the knee throughout the gait cycle. The highest functioning prosthetic ankles currently are carbon fiber springs that provide limited ankle motion and are aimed at returning a small portion of power to the gait cycle. It is the hypothesis of this work that the combination of actively powered knee and ankle joints with the capability

of generating human-scale net positive power can approach biomechanically normal gait in above knee amputees, and thus, increase their gait efficiency. In addition, reducing the effort required in daily ambulation activities to increase their quality of life.



Figure 1-1. State-of-the-art commercially available microprocessor knees include Ossur's Rheo Knee (left), the Otto Bock's C-Leg (center), and Freedom Innovations' Plié knee (right).

Literature Survey

Some of the earliest work in powered transfemoral prostheses was conducted during 1970's and 1980's and is described in [12-18]. Specifically, Flowers et. al. built an electro-hydraulically actuated knee joint which was tethered to a hydraulic power source and utilized off-board electronics and computation and was tested on at least one amputee subject. The gait control of the actuated knee utilized an "echo control" scheme [16]. In this control approach, the modified knee trajectory from the sound leg was used as a desired knee joint angle trajectory on the contralateral side. Prior work by Popovic and Schwirtlich reported on the development of an active knee joint actuated by DC motors and utilized a finite state knee controller with robust position tracking control for gait control [19], Fig. 1-2. Ossur, a prosthetics company, has recently introduced the "Power Knee" , Fig. 1-2, that uses a control approach, which like echo control,

utilizes inertial sensors on the sound leg to prescribe a trajectory for the knee joint of the prosthesis [20]. In [21], Martinez-Villalpando et. al. discuss a biomimetic prosthesis with an agonist-antagonist knee design that proposes to leverage the passive dynamics of normal gait, Fig. 1-2.

Figure 1-2. Powered knees developed by Popovic et. al. (left), Ossur (center) and Martinez-Villalpando et. al. (right).

Recent works in powered transtibial prostheses include work by Klute et. al., which describes the design of an active ankle joint using McKibben pneumatic actuators [22]. The prosthetics company, Ossur, has also introduced a “powered” ankle prosthesis, called the “Proprio Foot,” which does not contribute net power to gait, but rather quasistatically adjusts the ankle angle to avoid stumbling and to better accommodate sitting [23]. Bellman et al. describe an active robotic ankle prosthesis with two actuated degrees of freedom [24], Fig. 1-3. Au and Herr built a powered ankle-foot prosthesis that incorporates both parallel and series elasticity to reduce peak motor torque requirements and to increase bandwidth [25], Fig. 1-3.

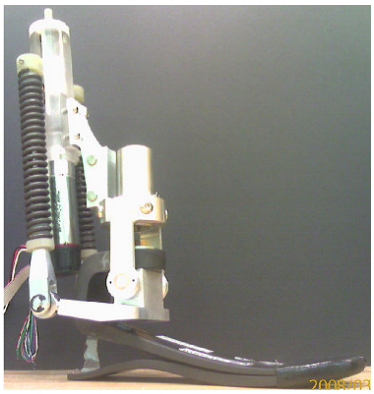

Figure 1-3. Prototype powered ankles developed by Bellman et. al. (left) and Au and Herr (right).

Unlike any of the aforementioned prior works, the author [26] describes a transfemoral prosthesis that combines both a powered knee and ankle to restore mobility. The tethered pneumatically powered device, Fig. 1-4, served as a laboratory test bed to develop the fundamental specifications and control for a powered knee and ankle prosthesis. In this paper, the concept of a finite-state impedance based gait controller is developed based on the use of passive impedance functions that coordinates the motion of the prosthesis with the user during level walking.

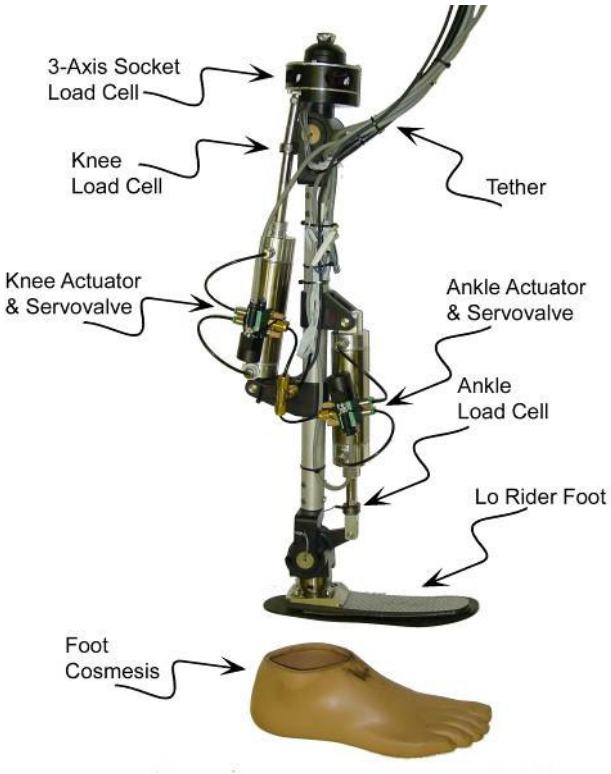

Figure 1-4. Pneumatically powered tethered prototype knee and ankle prosthesis previously developed by the author.

Scope and Summary of Research

This dissertation marks the transition from the author's previous work in pneumatically powered knee and ankle prostheses to electrically powered devices. In the previous work described in [26], the author developed a pneumatically powered knee and ankle prosthesis prototype designed to leverage the recent advances in monopropellant based pneumatic actuation described in [27-30]. Despite the advantages, monopropellant technology, in its current state, is not ready for commercialization in the near-term. In order to provide a technology that is more appropriate for near-term use, lithium-polymer batteries were chosen. Such batteries have an energy density approaching 200 W·h/kg [31], which as described herein, enables the development of a transfemoral prosthesis with a reasonable weight and an acceptable, although limited,

range of locomotion. The energy density of such batteries is expected to nearly double in the next decade (driven largely by the automotive industry's needs for electrical vehicles) [31], which will provide a significantly improved range of locomotion. Prior to developing a self-contained powered knee and ankle prosthesis, a tethered electrical powered knee and ankle prototype was built to explore the electrical power requirements of such a device. Subsequently, a self-contained version of a powered knee and ankle prosthesis was developed based on the specifications determined by the tethered prototype. Development of the device included the mechanical design of the device, actuation assemblies, sensor package, embedded electronics system, and a control strategy. The control of the device was refined to simplify the finite-state impedance control structure for gait, accommodate varied speeds and incorporate non-gait modes such as standing, sitting and the transitions between standing and sitting. Testing of the device was performed via an able-bodied adapter for initial debugging and parameter tuning. Final testing was performed with a single unilateral transfemoral amputee demonstrating the device on a treadmill and over normal ground as well as slope ascent, standing, sitting and sit-to-stand transition modes.

Organization of the Document

The dissertation is organized in six chapters. Chapter I presents the introduction and scope of the work. The chapters II to IV are comprised of the manuscripts that encompass the body of the work completed and have been submitted for publication as journal or conference papers. Chapter V presents the control structure for slope ascent and test results with the self-contained prosthesis on a unilateral transfemoral amputee. Chapter VI concludes with the contributions and future direction of the work. Overviews of the manuscripts presented in this dissertation are as follows:

Manuscript 1: Design and Control of an Active Electrical Knee and Ankle Prosthesis

This paper presents an overview of the design and control of a tethered electrically powered knee and ankle prosthesis. This prototype represents the transition point in the overall project from a pneumatically powered knee and ankle prosthesis to electric. The tethered prototype was developed to validate the electrically powered knee and ankle prosthesis concept and migrate the power source from pneumatic to an electric. The work demonstrates the capabilities of the device via an able-bodied adapter that allows the device to be worn by normal subjects. Projections from the study predicted reasonable power and energy requirements for a self-contained electrical device supporting the development of a self-contained version. Manuscript 1 is based on the following paper:

- F. Sup, H. A. Varol, J. Mitchell, T.J. Withrow, M. Goldfarb, "Design and Control of an Active Electrical Knee and Ankle Prosthesis," *Proc. IEEE/RAS-EMBS Int. Conf. on Biomedical Robotics and Biomechatronics* , pp. 523-528, 2008.

Manuscript 2: Preliminary Evaluations of a Self-Contained Anthropomorphic Transfemoral Prosthesis

In this work, the detailed description and testing of an electrical self-contained powered knee and ankle prosthesis are presented. The paper provides an overview of the main components of the prosthesis, including the mechanical design, sensor development, embedded system, control architecture and prototype testing. The prosthesis and control scheme are validated on a unilateral transfemoral amputee. Experimental results are shown that demonstrate the ability to restore biomimetic gait patterns on the prosthetic side and provide net power generation at the ankle over the gait cycle.

- F. Sup, H.A. Varol, and M. Goldfarb, "Preliminary Evaluations of a Self-Contained Anthropomorphic Transfemoral Prosthesis," *IEEE/ASME Transactions on Mechatronics*, 2009. Accepted.

Manuscript 3: Powered Sit-to-Stand and Assistive Stand-to-Sit Framework For a Powered Transfemoral

Prosthesis

This work presents a control framework for powered knee and ankle prosthesis during sitting and standing and the transitions between the two states. Expanding the general control framework presented in Manuscript 2, sitting, standing, powered sit-to-stand and assistive stand-to-sit are accomplished. The control structure is implemented on the self-contained prosthesis presented in Manuscript 2 and tested on a unilateral transfemoral amputee. Manuscript 3 is based on the following paper:

- H. A. Varol, F. Sup, and M. Goldfarb, "Powered Sit-to-Stand and Assistive Stand-to-Sit Framework for a Powered Transfemoral Prosthesis," *IEEE 11th International Conference on Rehabilitation Robotics*, pp. 645-651, 2009.

References

[1] P. F. Adams, G. E. Hendershot, and M. A. Marano, "Current estimates from the National Health Interview Survey, 1996," *National Center for Health Statistics. Vital Health Stat 10(200)*, 1999.

[2] J. Feinglass, J. L. Brown, A. LaSasso, M. W. Sohn, L. M. Manheim, S. J. Shah, and W. H. Pearce, "Rates of lower-extremity amputation and arterial reconstruction in the United States, 1979 to 1996," *American J. of Public Health,* vol. 89, no. 8, pp. 1222-1227, Aug, 1999.

[3] P. DeVita, M. Torry, K. L. Glover, and D. L. Speroni, "A functional knee brace alters joint torque and power patterns during walking and running," *J. of Biomechanics,* vol. 29, no. 5, pp. 583-588, May, 1996.

[4] R. Jacobs, M. F. Bobbert, and G. J. van Ingen Schenau, "Mechanical output from individual muscles during explosive leg extensions: The role of biarticular muscles," *J. of Biomechanics,* vol. 29, no. 4, pp. 513-523, Apr, 1996.

[5] S. Nadeau, B. J. McFadyen, and F. Malouin, "Frontal and sagittal plane analyses of the stair climbing task in healthy adults aged over 40 years: what are the challenges compared to level walking?," *Clinical Biomechanics,* vol. 18, no. 10, pp. 950-959, Dec, 2003.

[6] A. Nagano, Y. Ishige, and S. Fukashiro, "Comparison of new approaches to estimate mechanical output of individual joints in vertical jumps," *J. of Biomechanics,* vol. 31, no. 10, pp. 951-955, Oct, 1998.

[7] B. I. Prilutsky, L. N. Petrova, and L. M. Raitsin, "Comparison of mechanical energy expenditure of

joint moments and muscle forces during human locomotion," *J. of Biomechanics,* vol. 29, no. 4, pp. 405-415, Apr, 1996.

[8] R. Riener, M. Rabuffetti, and C. Frigo, "Joint powers in stair climbing at different slopes," *Proc. of the First Joint BMES/EMBS Conf.,* vol. 1, pp. 530 vol.1, 1999.

[9] D. Winter, *The Biomechanics and Motor Control of Human Gait: Normal, Elderly and Pathological*, 2nd ed.: University of Waterloo Press, 1991.

[10] D. A. Winter, and S. E. Sienko, "Biomechanics of below-knee amputee gait," *J. of Biomechanics,* vol. 21, no. 5, pp. 361-367, 1988.

[11] R. L. Waters, J. Perry, D. Antonelli, and H. Hislop, "Energy cost of walking of amputees - Influence of level of amputation," *J. of Bone and Joint Surgery-American Vol.,* vol. 58, no. 1, pp. 42-46, 1976.

[12] M. Donath, "Proportional EMG control for above knee prostheses," Massachusetts Institute of Tech. Dept. of Mechanical Eng. Thesis. M.S., 1974.

[13] W. C. Flowers, "A man-interactive simulator system for above-knee prosthetics studies," Massachusetts Institute of Tech. Dept. of Mechanical Eng. Thesis. Ph.D., 1973.

[14] W. C. Flowers, and R. W. Mann, "Electrohydraulic knee-torque controller for a prosthesis simulator," *ASME J. of Biomechanical Engineering,* vol. 99, no. 4, pp. 3-8, 1977.

[15] D. L. Grimes, "An active multi-mode above knee prosthesis controller," Massachusetts Institute of Tech. Dept. of Mechanical Eng. Thesis Ph.D., 1979.

[16] D. L. Grimes, W. C. Flowers, and M. Donath, "Feasibility of an active control scheme for above knee prostheses," *ASME J. of Biomechanical Engineering,* vol. 99, no. 4, pp. 215-221, 1977.

[17] J. L. Stein, and W. C. Flowers, "Stance phase-control of above-knee prostheses - Knee control versus SACH foot design," *J. of Biomechanics,* vol. 20, no. 1, pp. 19-28, 1987.

[18] J. L. Stein, and Massachusetts Institute of Technology. Dept. of Mechanical Engineering., "Design issues in the stance phase control of above-knee prostheses," Massachusetts Institute of Tech. Dept. of Mechanical Eng. Thesis Ph.D., 1983.

[19] D. Popovic, and L. Schwirtlich, "Belgrade active A/K prosthesis," *in de Vries, J. (Ed.), Electrophysiological Kinesiology, Intern. Congress Ser. No. 804, Excerpta Medica, Amsterdam, The Netherlands*, pp. 337-343, 1988.

[20] S. Bedard, and P. Roy, *Actuated leg prosthesis for above-knee amputees*, 7,314,490, U. S. Patent, June 17, 2003.

[21] E. Martinez- Villalpando, J. Weber, G. Elliott, and H. Herr, “Design of an agonist-antagonist active knee prosthesis,” *Proc. IEEE/RAS-EMBS Int. Conf. on Biomedical Robotics and Biomechatronics*, pp. 529-534, 2008.

[22] G. K. Klute, J. Czerniecki, and B. Hannaford, “Muscle-like pneumatic actuators for below-knee prostheses,” *Proc. 7th Int. Conf. on New Actuators*, pp. 289-292, 2000.

[23] W. Koniuk, *Self-adusting prosthetic ankle apparatus*, 6,443,993, U. S. Patent, March, 23, 2001.

[24] R. Bellman, A. Holgate, and T. Sugar, “SPARKy 3: Design of an active robotic ankle prosthesis with two actuated degrees of freedom using regenerative kinetics,” *Proc. IEEE/RAS-EMBS Int. Conf. on Biomedical Robotics and Biomechatronics*, pp. 511-516, 2008.

[25] S. Au, and H. Herr, “Powered ankle-foot prosthesis,” *IEEE Robotics & Automation Magazine,* vol. 15, pp. 52-59, 2008.

[26] F. Sup, A. Bohara, and M. Goldfarb, “Design and control of a powered transfemoral prosthesis,” *Int. J. of Robotics Research,* vol. 27, no. 2, pp. 263-273, Feb, 2008.

[27] K. B. Fite, and M. Goldfarb, “Design and energetic characterization of a proportional-injector monopropellant-powered actuator,” *IEEE/ASME Trans. on Mechatronics,* vol. 11, no. 2, pp. 196-204, Apr, 2006.

[28] K. B. Fite, J. E. Mitchell, E. J. Barth, and M. Goldfarb, “A unified force controller for a proportional-injector direct-injection monopropellant-powered actuator,” *J. of Dynamic Systems Measurement and Control Trans. of ASME,* vol. 128, no. 1, pp. 159-164, Mar, 2006.

[29] M. Goldfarb, E. J. Barth, M. A. Gogola, and J. A. Wehrmeyer, “Design and energetic characterization of a liquid-propellant-powered actuator for self-powered robots,” *IEEE/ASME Trans. on Mechatronics,* vol. 8, no. 2, pp. 254-262, 2003.

[30] B. L. Shields, K. B. Fite, and M. Goldfarb, “Design, control, and energetic characterization of a solenoid-injected monopropellant-powered actuator,” *IEEE/ASME Trans. on Mechatronics,* vol. 11, no. 4, pp. 477-487, Aug, 2006.

[31] “In search of the perfect battery,” *Economist,* vol. 386, no. 8570, pp. 22-24, 2008.

CHAPTER II

Manuscript 1: Design and Control of an Active Electrical Knee and Ankle Prosthesis

Frank Sup,

Huseyin Atakan Varol, Jason Mitchell, Thomas J. Withrow and Michael Goldfarb

Vanderbilt University

Nashville, TN

Accepted as a Technical Paper to the

Proceedings of the 2008 IEEE/RAS-EMBS International Conference on

Biomedical Robotics and Biomechatronics

Abstract

This paper presents an overview of the design and control of an electrically powered knee and ankle prosthesis. The prosthesis design incorporates two motor-driven ball screw units to drive the knee and ankle joints. A spring in parallel with the ankle motor unit is employed to decrease the power consumption and increase the torque output for a given motor size. The device's sensor package includes a custom load cell to measure the sagittal socket interface moment above the knee joint, a custom sensorized foot to measure the ground reaction force at the heel and ball of the foot, and commercial potentiometers and load cells to measure joint positions and torques. A finite-state based impedance control approach, previously developed by the authors, is used and experimental results on level treadmill walking are presented that demonstrate the potential of the device to restore normal gait. The experimental power consumption of the device projects a walking distance of 5.0 km at a speed of 2.8 km/hr with a lithium polymer battery pack.

Introduction

The native limb generates significant net power over a gait cycle in many locomotive functions including walking, walking up stairs and slopes, running and jumping [1-8]. In the absence of net power generation, transfemoral amputees with passive prosthesis have been shown to expend 60% more metabolic energy [9] and exert three times the affected-side hip power and torque [1] when compared to healthy subjects during level walking.

To the authors' knowledge, the earliest powered transfemoral prosthesis was developed at MIT during 1970's and 1980's [10-16]. This prosthesis consisted of an electro-hydraulically actuated knee joint tethered to a hydraulic power source and utilized off-board electronics and computation. As described in [13], an

"echo control" scheme was developed for gait control. In echo control, the modified knee trajectory from the sound leg is played back on the contralateral side. Popovic and Schwirtlich reported the development of an active knee joint actuated by DC motors [17]. They utilized a finite state knee controller with robust position tracking control for gait control. In [18], the design of an active ankle joint using McKibben pneumatic actuators is described. The feasibility of electromyography based position control approach for transtibial prosthesis is assessed in [19]. Although no scientific literature is available, Ossur, a prosthetics company, has recently made available a powered knee and a self-adjusting ankle. The "Power Knee" uses a control approach similar to echo control, which utilizes sensors on the sound leg. The Ossur powered ankle prosthesis, called the "Proprio Foot", does not contribute net power to gait, but rather quasi-statically adjusts the ankle angle to optimize gait.

The authors have developed a pneumatically powered knee and ankle prosthesis prototype, in which they used finite state-based impedance control that only utilizes sensors on the prosthesis itself [20]. This prototype was built to take advantage of the recent advances in monopropellant based pneumatic actuation described by [21-24]. The authors believe that the monopropellant technology in its current state is not ready for commercialization in the near-term. Current lithium-polymer batteries have an energy density approaching 200 W·h/kg [25], which enable the development of a transfemoral prosthesis with a reasonable weight and an acceptable, although limited, range of locomotion. The energy density of such batteries is expected to nearly double in the next decade (driven largely by the automotive industry's needs for electrical vehicles) [25], which will provide a more generous range of locomotion.

In this paper, the authors describe progress toward the development of an electrically powered active knee and ankle prosthesis. This prosthesis will be able to generate human-scale power at the joints and

incorporate a torque-based control framework for stable and coordinated interaction between the prosthesis and the user. The paper describes the mechanical design of the prosthesis, provides an overview of the finite-state based impedance control framework, presents experimental results on a healthy subject using an able-bodied adapter, and discusses the electrical power requirements in different gait modes.

Design Specifications

Prosthesis Prototype

The active joint torque specifications were based on an 85 kg user for fast walking and stair climbing, as derived from body-mass-normalized data [1, 3]. The prosthesis is capable of 90° of flexion at the knee and 45° of planterflexion and 20° of dorsiflexion at the ankle. The electric powered prosthesis prototype is presented in a labeled photograph, Fig. 1. The prosthesis is actuated by two motor-driven ball screw assemblies that drive the knee and ankle joints, respectively, through a slider-crank linkage. Each actuation unit consists of a Maxon motor (Model 148867) capable of producing 150 W of continuous power connected to a 2mm lead ball screw of 10 mm and 12 mm diameters for the knee and ankle, respectively, via Oldham couplings.

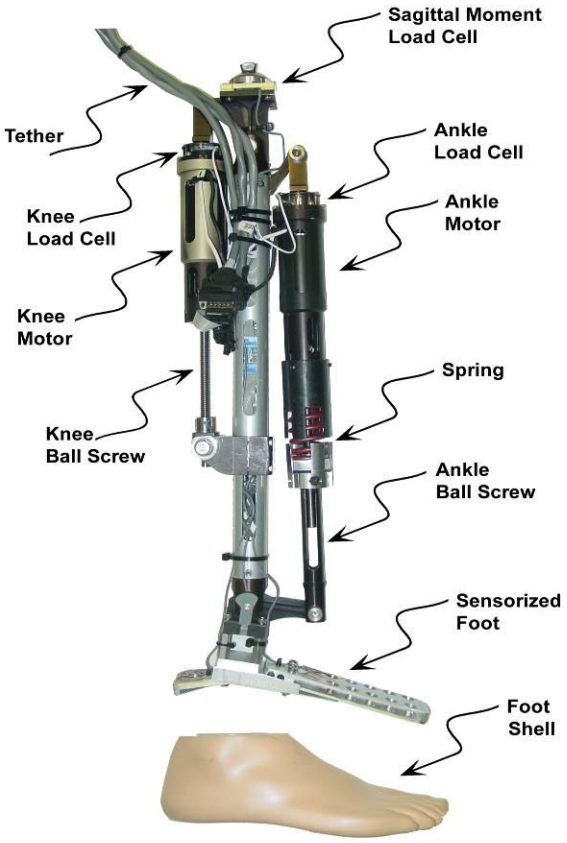

Figure 2-1. The power tethered prototype.

The ankle actuation unit additionally incorporates a spring of stiffness 1100 N/cm in parallel with the ball screw, the purpose of which is to bias the motor's axial force output toward ankle plantarflexion, and to supplement power output during ankle push off. The resulting axial actuation unit's force versus ankle angle plot, Fig. 2-2, graphically demonstrates for fast walking the reduction in linear force output supplied by the motor at the ankle through the addition of the spring. Note that the compression spring does not engage until approximately five degrees of ankle plantarflexion. Each actuation unit additionally includes a uniaxial load cell (Measurement Specialties ELPF-500L), positioned in series with the motor for force control. Both the knee and ankle joints incorporate composite plain bearings (Garlock model DU) and, for joint angle measurement, integrated precision potentiometers (ALPS RDC503013). A strain based

sagittal plane moment sensor, Fig. 2-3, is located between the knee joint and the socket connector, which measures the moment between the socket and prosthesis. The ankle joint connects to a custom foot design, Fig. 2-4, which incorporates strain gages to measure the ground reaction forces on the ball of the foot and on the heel. The present prototype houses onboard signal conditioning electronics and relies on a tether for power, computation and power electronics.

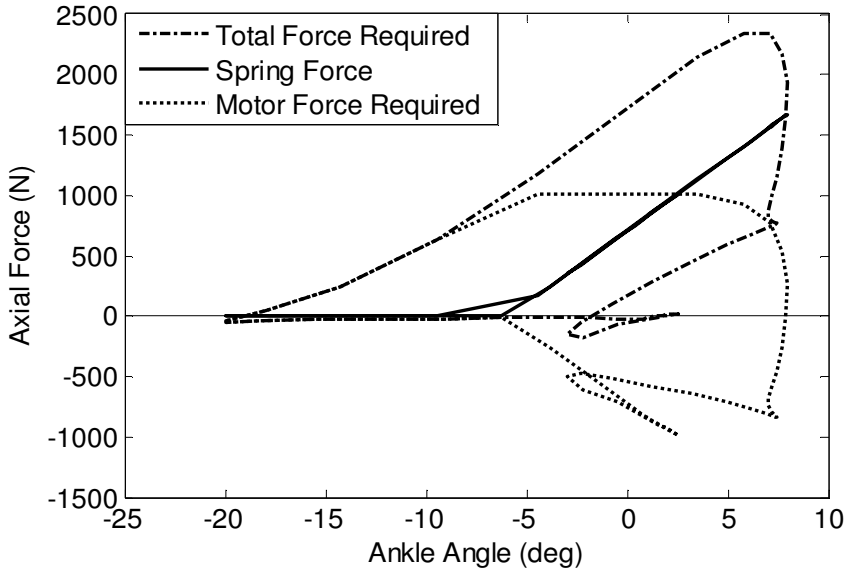

Figure 2-2. The reduction of linear force output required by the ankle motor unit by the addition of a spring in parallel for fast walking, taken from averaged normal biomechanical data [1].

Figure 2-3. Sagittal moment load cell, top and bottom views.

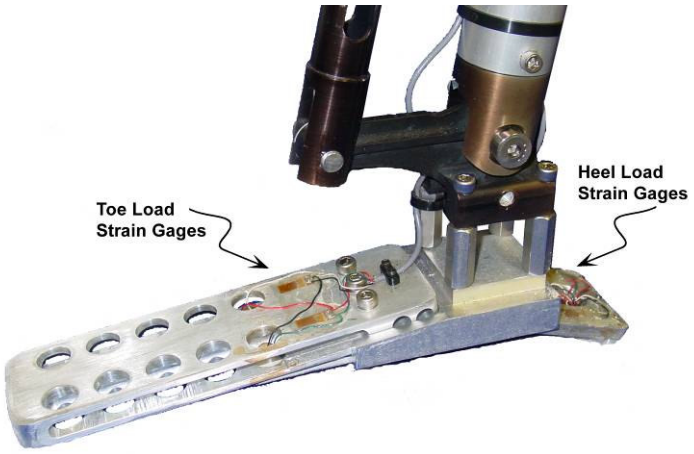

Figure 2-4. Sensorized prosthetic foot.

The knee height of device is varied by changing the main structural tube and the clamping supports for the knee actuation unit and ankle spring. Additionally, the ankle joint and the sagittal moment load cell incorporate standard pyramid connectors for coupling the prosthesis to the foot and socket, thus enabling a high degree of adjustment in the knee and ankle alignment, as is standard in transfemoral prostheses. Combined with the custom sensorized foot (0.35 kg) and foot shell (0.24 kg) the total weight of the tethered transfemoral prosthesis is 3.8 kg, which is within an acceptable range for transfemoral prostheses, and less than a comparable normal limb segment [26]. An untethered version incorporating batteries and on-board electronics is expected to weigh less than 4.5 kg with further structural weight savings.

Moment and Force Sensing

The load between the user and prosthesis, and between the prosthesis and ground, is sensed in order to infer user intent and enable prosthesis control. Based on the data presented in [1] and [4], the required range of measurements was determined to be 100 Nm of sagittal plane moment and a ground reaction force of 1000 N. The sagittal plane moment is measured above the knee joint at the socket interface and the ground reaction force is measured by the sensorized foot. The location of the sensors was chosen to

avoid coupling the desired measured ground reaction force and sagittal moment with the joint torques. In addition, incorporating the ground reaction load cell into the structure of a custom foot itself eliminates the added weight of a separate load cell.

The sagittal plane moment sensor shown in Fig. 2-3 is a low profile design to allow for the longest residual limb of the user. The mechanics of the design are based on a single beam in bending with a moment and force applied at the center. The design is a flat plate mounted on two supports on the edges parallel to the frontal plane. A central ridge along the top concentrates the load and adds rigidity to resist the frontal plane moments. On top of the central ridge is a platform that allows for a pyramid connector to be attached. Finite element analysis, using ProEngineer Mechanica, was used to minimize the overall design height and to achieve the desired strains in the load cell. The sensor was fabricated from 7075 aluminum and has an assembled weight of 120 grams including the stainless steel pyramid connector. The overall height of the sensor including the pyramid connector is 35 mm and the base is a 50 mm square. The device was calibrated for 100 Nm with ± 5% error at full state output.

A sensorized foot, Fig. 2-4, is used to measure the ground reaction force and is comprised of toe and heel beams rigidly attached to a central fixture. The toe and heel portions of the foot are arranged as cantilever beams with an arch that allows for the load to be localized at the ends. The device is fabricated of 7075 aluminum and weighs 350 grams. The foot fabricated for the test subject measures 220 mm long, 56 mm wide and is 35 mm tall to the top of the central fixture and approximates a US size 12 or EU size 46 foot. The overall dimensions and weight are similar to commercial low-profile carbon-fiber prosthetic feet, such as the Otto Bock Lo-Rider. The prosthetic foot was designed to be housed in a soft prosthetic foot shell (see Fig. 2-1). The device was calibrated for 1000 N with ± 4% error at full state output.

Control

The control approach developed by the authors utilizes an impedance-based approach to generate joint torques [20]. Generating torques rather then positions enables the user to interact with the prosthesis by leveraging its dynamics in a manner similar to normal gait, and also generates stable and predictable behavior. In the algorithm, the knee and ankle torques, τ_i , are characterized by Eqn. 1, with a series of finite states, Fig. 2-5, consisting of passive spring and damper behaviors,

$$\tau_i = -k_i(\theta - \theta_{ki}) - b_i\dot{\theta} \tag{1}$$

where k_i and b_i denote the linear stiffness and damping coefficient for an i^{th} state, respectively. Energy is delivered to the user by switching between appropriate equilibrium positions, θ_k, (of the virtual springs) during state transitions. In this manner, the prosthesis is guaranteed to be passive within each gait mode, and thus generates power simply by switching between modes. Since the user initiates mode switching, the result is a predictable controller that, barring mode switching input from the user, will always default to passive behavior.

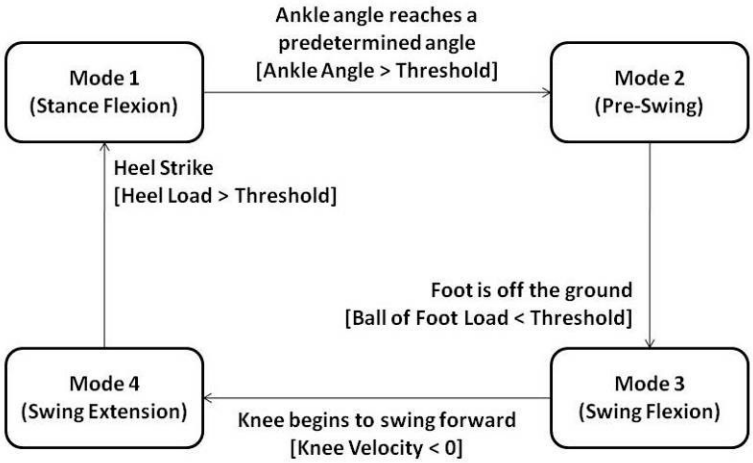

Figure 2-5. The finite state switching model for impedance control. Blocks represent a state and arrows represent the corresponding transitions.

Experimental Setup

The main components of the experimental setup consist of a tethered powered prosthesis and a treadmill. The powered prosthesis is tethered to two Kepco BOP 36-12D servo-amplifiers, and a laptop computer running MATLAB Real Time Workshop for controller implementation. In addition, current and voltage sensing circuitry is employed to measure the currents and voltages passing through the knee and ankle motors. The prosthesis is tested using an able-bodied adapter on a healthy male subject, who is 1.93 m tall and weighs 86 kg, as shown in Fig. 2-6.

Figure 2-6. Able-bodied testing adapter used in the development of the prosthesis and controllers prior to transfemoral amputee participation.

The prosthesis is tuned for the subject using the finite-state impedance approach for standing and for walking at three different walking speeds – slow, normal and fast (2.2, 2.8 and 3.4 km/hr). The parameters of the tuned modal impedance functions are presented in Tables 2-1 and 2-2. The current and voltage to

each motor and prosthesis sensor data are collected for each walking speed and standing on two separate trials lasting 100 seconds. During the standing mode, the test subject alternately shifted his weight between limbs, turned in place, and stood still. The prosthesis sensor data consists of joint positions, velocities and torques, socket sagittal plane moment and heel and ball of foot loads.

Table 2-1. Impedance parameters for walking from experimental tuning. Highlighted parameters vary with walking speed.

		Knee Impedance			Ankle Impedance		
Mode	Speed	k	b	θ_k	k	b	θ_k
	km h^{-1}	Nm deg^{-1}	N s m^{-1}	deg	Nm deg^{-1}	N s m^{-1}	deg
	2.2	1.5	0	10	3.5	0	-4.4*
1	2.8	1.5	0	13	3.5	0	-4.4*
	3.4	2.0	0	13	4.0	0	-4.4*
	2.2	1.5	0.05	16	3.5	0	-18
2	2.8	1.5	0.05	16	4.0	0	-19
	3.4	2.0	0.05	16	4.5	0	-20
	2.2	0	0.01	50	0.3	0.02	0
3	2.8	0	0.01	50	0.3	0.02	0
	3.4	0	0.01	50	0.3	0.02	0
	2.2	0	0.045	45	0.3	0	0
4	2.8	0	0.035	45	0.3	0	0
	3.4	0	0.04	45	0.3	0	0

* Equilibrium angle is a nonlinear function of knee and ankle angles. The listed value is the initial equilibrium set point.

Table 2-2. Impedance parameters for standing from experimental tuning.

Mode	Knee Impedance			Ankle Impedance		
	k Nm deg^{-1}	b N s m^{-1}	θ_k deg	k Nm deg^{-1}	b N s m^{-1}	θ_k deg
Ground Contact	2.0	0.05	5	5.0	0	-4
No Ground Contact	0	0.02	5	2.0	0	-4

Results and Discussion

Performance

Measured joint angles from the prosthesis' onboard sensors during level treadmill walking at 2.2, 2.8, and 3.4 km/hr are presented in Fig. 2-7. In comparing the knee and ankle angles to the prototypical data [1], one can observe that the powered prosthesis and controller provide behavior quite similar to normal gait. The knee and ankle torque trajectories with references are presented in Fig. 2-8, demonstrating capabilities of the electric prosthesis to produce the requisite forces.

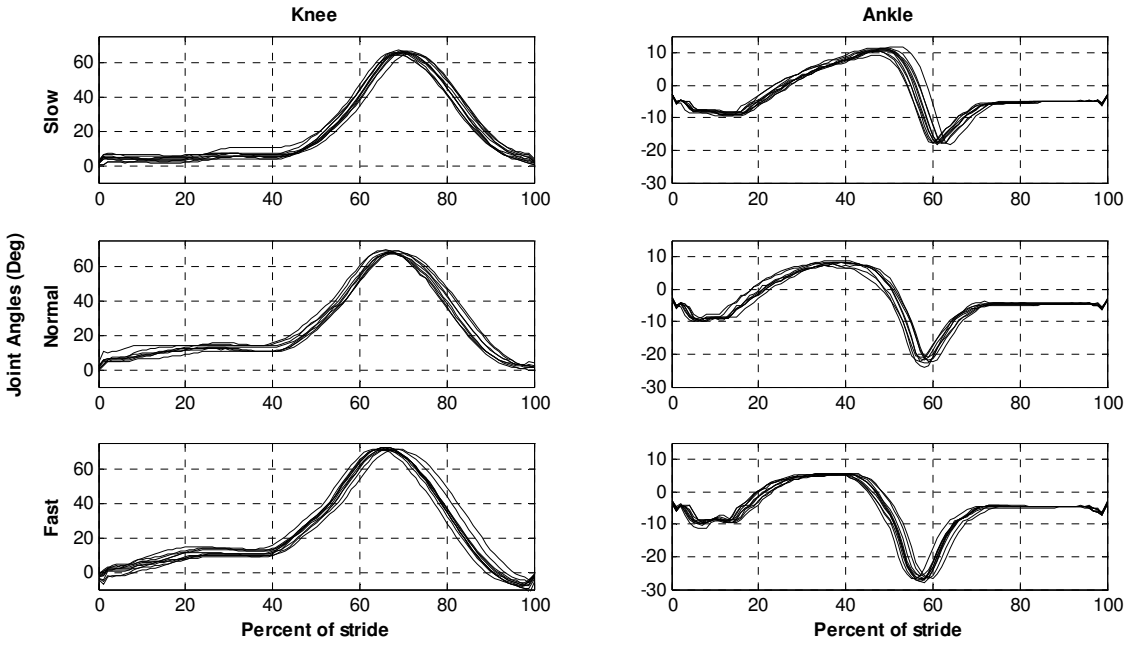

Figure 2-7. Measured joint angles of the powered prosthesis for ten consecutive gait cycles of treadmill walking at three different speeds - 2.2, 2.8, 3.4 km/hr.

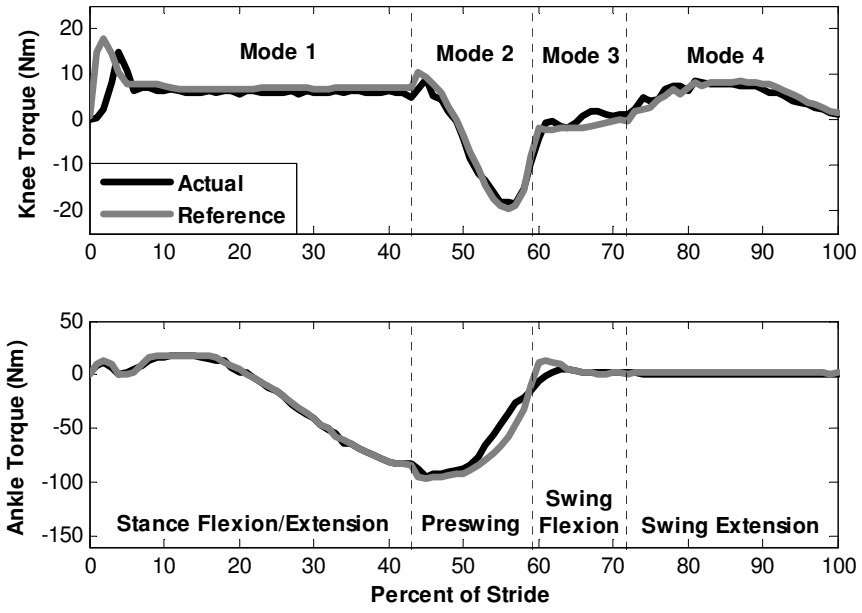

Figure 2-8. References and actual knee and ankle joint torques of the powered prosthesis for one stride at normal speed.

Power Consumption

One of the primary constraints of the electrical powered knee and ankle prosthesis design is the power source. As such, the power consumption of the prosthesis was assessed to characterize the feasibility of such as device in terms of mass and range. The power delivered at each joint during a slow walking trial is shown in Fig. 2-9. Fig. 2-10 shows the average mechanical power of the prosthesis for the various modes, along with the average electrical input power. As can be observed from the figure, the maximum average power consumption in the normal walking mode is about 65 Watts. It is assumed that high frequency switching servo-amplifiers with 90% efficiency will be used to drive the motors. Moreover, an additional 5 Watts is added for on-board signal conditioning and computation. Thus, it is estimated that normal walking will require approximately 77 Watts of average power. Finally, it is assumed that the prosthesis can accommodate approximately 600-700 grams of battery. Given these assumptions, Table 2-3 shows several lithium polymer battery options for the prosthesis, and the estimated walking distance in normal walking mode for the healthy experimental subject with the able-bodied adapter. As seen in the table, such an arrangement provides approximately 4.4-5.0 km of walking range. Given current projections of battery technology, this range should roughly double (to approximately 10 km) within the next decade.

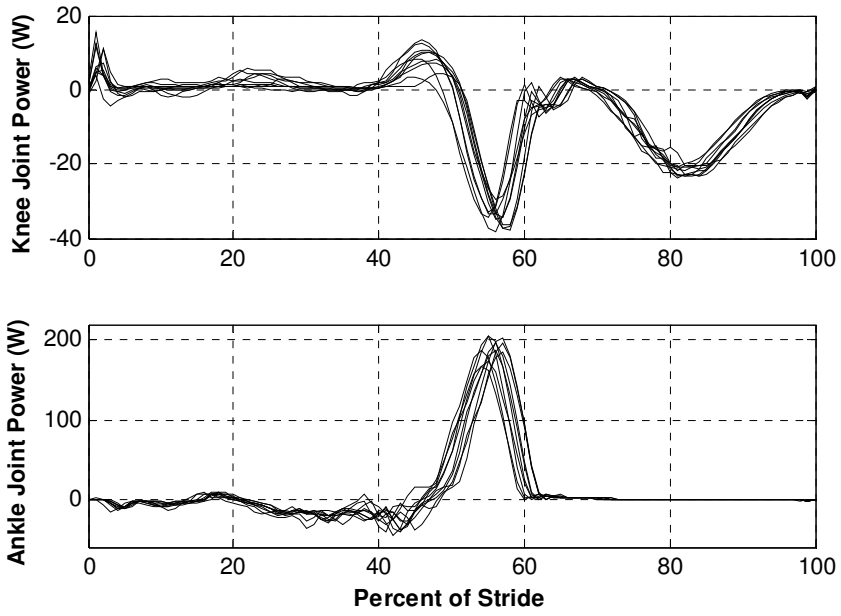

Figure 2-9. Measured mechanical power of the prosthesis for ten consecutive gait cycles of treadmill walking at slow speed.

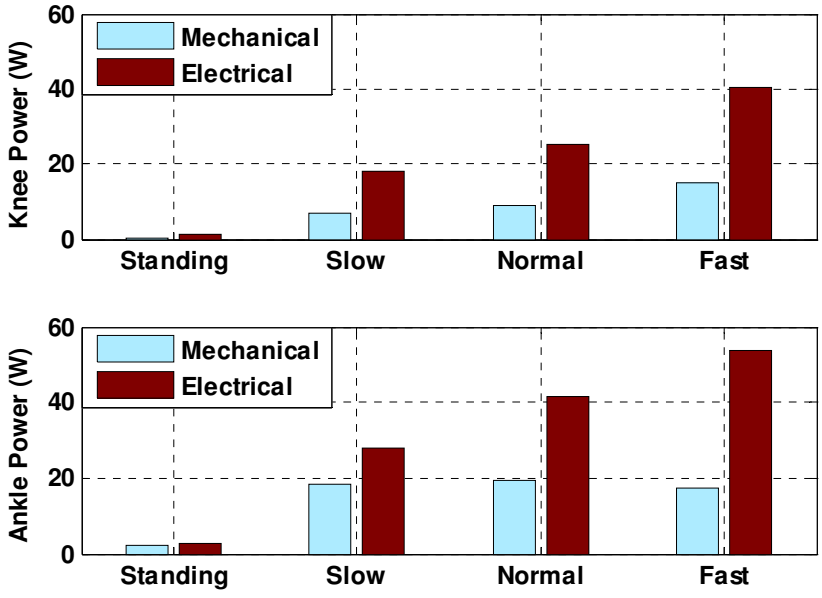

Figure 2-10. Average electrical power consumption and mechanical power generation at the ankle and knee of the powered prosthesis for standing and different walking speeds.

Table 2-3. Selected commercially available lithium polymer battery options and the walking distance at normal walking speed.

Option	Voltage (V)	Capacity (mA·h)	Energy (W·h)	Weight (gr)	Walking Distance (km)
1	29.6	4000	118.4	622	4.4
2	29.6	2000	118.4	640	4.4
3	33.3	2000	133.2	720	5.0

Conclusion and Further Works

The paper describes the design of an electrically powered knee and ankle prosthesis capable of producing human-scale power. Utilizing finite-state impedance based control and an able-bodied testing adapter, experimental results were obtained to demonstrate the merit of the device and measure its power consumption. With current battery technology the prosthesis range is 5.0 km at a normal walking speed, which is projected to double within the next decade. Future work includes testing the powered prosthesis on amputee subjects and implementing a self-contained version with on-board servo-amplifiers, batteries and computational capabilities.

References

[1] Winter, D.A. The biomechanics and motor control of human gait: normal, elderly and pathological, University of Waterloo Press, 2nd edition, 1991.

[2] Winter, D. A. and Sienko, S. E. Biomechanics of below-knee amputee gait. J. Biomechanics. 21, 361–367, 1988.

[3] Nadeau, S., McFadyen, B.J., and Malouin, F. Frontal and sagittal plane analyses of the stair climbing task in healthy adults aged over 40 years: What are the challenges compared to level walking? Clinical Biomechanics, vol. 18, no. 10, pp. 950-959, 2003.

[4] Riener, R., Rabuffetti, M., and Frigo, C. Joint powers in stair climbing at different slopes. Proceedings of the IEEE International Conference on Engineering in Medicine and Biology, vol. 1, p. 530, 1999.

[5] Prilutsky, B.I., Petrova, L.N., and Raitsin, L.M. Comparison of mechanical energy expenditure of joint moments and muscle forces during human locomotion. Journal of Biomechanics, vol. 29, no. 4, pp. 405-415, 1996.

[6] DeVita, P., Torry M., Glover, K.L., and Speroni, D.L. A Functional Knee Brace Alters Joint Torque and Power Patterns during Walking and Running, Journal of Biomechanics, vol. 29, no. 5, pp. 583-588, 1996.

[7] Nagano, A., Ishige, Y., and Fukashiro, S. Comparison of new approaches to estimate mechanical output of individual joints in vertical jumps. Journal of Biomechanics, vol. 31, no. 10, pp. 951-955, 1998.

[8] Jacobs, R., Bobbert, M.F., van Ingen Schenau, G.J. Mechanical output from individual muscles during explosive leg extensions: the role of biarticular muscles. Journal of Biomechanics, vol. 29, no. 4, pp. 513-523, 1996.

[9] Waters, R., Perry, J., Antonelli, D., and Hislop, H. Energy cost of walking amputees: the influence of level of amputation. J. Bone and Joint Surgery. 58A, 42–46, 1976.

[10] Flowers, W.C., A Man-Interactive Simulator System for Above-Knee Prosthetics Studies, Department of Mechanical Engineering PhD Thesis, MIT, 1973.

[11] Donath, M., Proportional EMG Control for Above-Knee Prosthesis', Department of Mechanical Engineering Masters Thesis, MIT, 1972.

[12] Grimes, D. L. An Active Multi-Mode Above Knee Prosthesis Controller. Department of Mechanical Engineering PhD Thesis, MIT, 1979.

[13] Grimes, D. L., Flowers, W. C., and Donath, M. Feasibility of an active control scheme for above knee prostheses. ASME Journal of Biomechanical Engineering, vol. 99, no. 4, pp. 215-221, 1977.

[14] Stein, J.L. Design Issues in the Stance Phase Control of Above-Knee Prostheses. Department of Mechanical Engineering PhD Thesis, MIT, 1983

[15] Stein, J.L., and Flowers, W.C. Stance phase control of above-knee prostheses: knee control versus SACH foot design. Journal of Biomechanics, vol. 20, no. 1, pp. 19-28, 1987.

[16] Flowers, W.C., and Mann, R.W. Electrohydraulic knee-torque controller for a prosthesis simulator. ASME Journal of Biomechanical Engineering, vol. 99, no. 4, pp. 3-8, 1977.

[17] Popovic, D. and Schwirtlich, L. Belgrade active A/K prosthesis, in de Vries, J. (Ed.), Electrophysiological Kinesiology, Intern. Congress Ser. No. 804, Excerpta Medica, Amsterdam, The Netherlands, pp. 337–343, 1988.

[18] Klute, G.K., Czerniecki, J., Hannaford, B., "Muscle-Like Pneumatic Actuators for Below-Knee Prostheses, Proceedings the Seventh Int. Conf. on New Actuators, pp. 289–292, 2000.

[19] Au, S. ,Bonato, P., Herr, H., "An EMG-Position Controlled System for an Active Ankle-Foot Prosthesis: An Initial Experimental Study," Proceedings of the IEEE Int. Conf. on Rehabilitation Robotics, pp. 375-379, 2005.

[20] Sup, F., Bohara, A., Goldfarb, M., “Design and Control of a Powered Transfemoral Prosthesis,” The International Journal of Robotics Research, pp. 263-273, vol. 27, Feb 2008.

[21] Goldfarb, M., Barth, E.J., Gogola, M.A. and Wehrmeyer, J.A., "Design and Energetic Characterization of a Liquid-Propellant-Powered Actuator for Self-Powered Robots," IEEE/ASME Trans. on Mechatronics, vol. 8, no. 2, pp. 254-262, 2003.

[22] Shields, B.L., Fite, K., and Goldfarb, M., “Design, Control, and Energetic Characterization of a Solenoid Injected Monopropellant Powered Actuator,” IEEE/ASME Trans. on Mechatronics, vol. 1, no. 4, pp. 477-487, 2006.

[23] Fite, K.B., Mitchell, J., Barth, E.J., and Goldfarb, M. A Unified Force Controller for a Proportional-Injector Direct-Injection Monopropellant-Powered Actuator, ASME J. of Dynamic Systems, Measurement and Control, vol. 128, no. 1, pp. 159-164, 2006.

[24] Fite, K.B., and Goldfarb, M., “Design and Energetic Characterization of a Proportional-Injector Monopropellant-Powered Actuator,” IEEE/ASME Trans. on Mechatronics, vol. 11, no. 2, pp. 196-204, 2006.

[25] In Search of the perfect battery, Economist, vol. 386, no. 8570, pp. 22-24, 2008.

[26] Clauser CE, McConville JT, Young JM, “Weight, volume and center of mass of segments of the human body.” AMRL-TR-69-70, Wright Patterson Airforce Base, Dayton, Ohio, 1969.

CHAPTER III

Manuscript 2: Preliminary Evaluations of a Self-Contained Anthropomorphic Transfemoral Prosthesis

Frank Sup,

Huseyin Atakan Varol, Jason Mitchell, Thomas J. Withrow and Michael Goldfarb

Vanderbilt University

Nashville, TN

Accepted as a Regular Paper to the

IEEE/ASME Transactions on Mechatronics

in the focused section

Anthropomorphism in Mechatronic Systems

Abstract

This paper presents a self-contained powered knee and ankle prosthesis, intended to enhance the mobility of transfemoral amputees. A finite-state based impedance control approach, previously developed by the authors, is used for the control of the prosthesis during walking and standing. Experiments on an amputee subject for level treadmill and overground walking are described. Knee and ankle joint angle, torque, and power data taken during walking experiments at various speeds demonstrate the ability of the prosthesis to provide a functional gait that is representative of normal gait biomechanics. Measurements from the battery during level overground walking indicate that the self-contained device can provide over 4,500 strides, or 9 km, of walking at a speed of 5.1 km/h between battery charges.

Introduction

There are more than 300,000 transfemoral amputees [1] in the United States (i.e., an incidence of approximately one per thousand people), with 30,000 new transfemoral amputations conducted each year [2]. If similar trends hold across the world population, then one would expect approximately 7 million transfemoral amputees worldwide. One of the most significant limitations of current prosthetic technology is the inability to provide net power at the joints. This loss of net power generation at the lower limb impairs the ability of the prosthesis to restore biomechanically normal locomotive function during many locomotive activities, including level walking, walking up stairs and slopes, running and jumping [3-10]. In the absence of net power generation at the knee and ankle, transfemoral amputees with passive prostheses have been shown to expend 60% more metabolic energy [11] and exert three times the affected-side hip power and

torque [9] when compared to healthy subjects during level walking. It is the hypothesis of this work that an actively powered knee and ankle prosthesis with the capability of generating human-scale net positive power over a gait cycle will provide improved functional restoration relative to passive prostheses.

Some of the earliest work in powered transfemoral prostheses was conducted during 1970's and 1980's and is described in [12-18]. Specifically, an electro-hydraulically actuated knee joint, which was tethered to a hydraulic power source and utilized off-board electronics and computation, was developed and tested on at least one amputee subject. As described in [16], an "echo control" scheme was developed for gait control. In this control approach, the modified knee trajectory from the sound leg was used as a desired knee joint angle trajectory on the contralateral side. Other prior work reported the development of an active knee joint actuated by DC motors and utilized a finite state knee controller with robust position tracking control for gait control [19]. Ossur, a prosthetics company, has recently introduced the "Power Knee" that uses a control approach, which like echo control, utilizes sensors on the sound leg to prescribe a trajectory for the knee joint of the prosthesis [20]. In [21], the authors discuss a biomimetic prosthesis with an agonist-antagonist knee.

Work in powered transtibial prostheses includes [22], which describes the design of an active ankle joint using McKibben pneumatic actuators. Ossur has also introduced a "powered" ankle prosthesis, called the "Proprio Foot," which does not contribute net power to gait, but rather quasistatically adjusts the ankle angle to avoid stumbling and to better accommodate sitting [23]. Bellman et al. describe an active robotic ankle prosthesis with two actuated degrees of freedom [24]. Au and Herr built a powered ankle-foot prosthesis that incorporates both parallel and series elasticity to reduce peak motor torque requirements and to increase bandwidth [25].

Unlike any of the aforementioned prior works, this paper describes a transfemoral prosthesis with both a powered knee and ankle. Note that, as described by Sup et al. [26], the authors have developed previously a pneumatically powered knee and ankle prosthesis prototype, which was designed to leverage recent advances in monopropellant based pneumatic actuation described [27-30]. Despite this, the authors believe that the monopropellant technology in its current state is not ready for commercialization in the near-term. In order to provide a technology that is more appropriate for near-term use, the authors describe in this paper a powered knee and ankle prosthesis powered by a lithium-polymer battery. Such batteries have an energy density approaching 200 W·h/kg [31], which as described herein, enables the development of a transfemoral prosthesis with a reasonable weight and an acceptable, although limited, range of locomotion. The energy density of such batteries is expected to nearly double in the next decade (driven largely by the automotive industry's needs for electrical vehicles) [31], which will provide a significantly improved range of locomotion. Prior to developing the self-contained, battery-powered powered knee and ankle prosthesis described herein, Sup et al. [32] previously built a tethered electrical powered knee and ankle prototype to explore the electrical power requirements of such a device.

Based on this preliminary work, the authors have developed an electrically powered self-contained active knee and ankle prosthesis, which is described herein. The self-contained prosthesis generates human-scale power at the joints and incorporates a torque-based control framework for stable and coordinated interaction between the prosthesis and the user. This paper describes the mechanical and electrical design of the prosthesis, provides an overview of the finite-state based impedance control framework for walking and standing, presents experimental results on a single transfemoral amputee subject, and discusses the electrical power requirements in different activity modes.

Prosthesis Design

The joint torque specifications required of the knee and ankle joints were based on an 85 kg user for a walking cadence of 80 steps per minute, Fig. 3-1, and stair climbing, as derived from body-mass-normalized data [8, 9], while the joint power specifications were based on data from Winter [9], also for an 85 kg user. The design specifications are summarized in Table 3-1. The resulting self-contained powered knee and ankle prosthesis is shown in Fig. 3-2. A detailed discussion of the mechanical, sensor and embedded system design is given in the following sections.

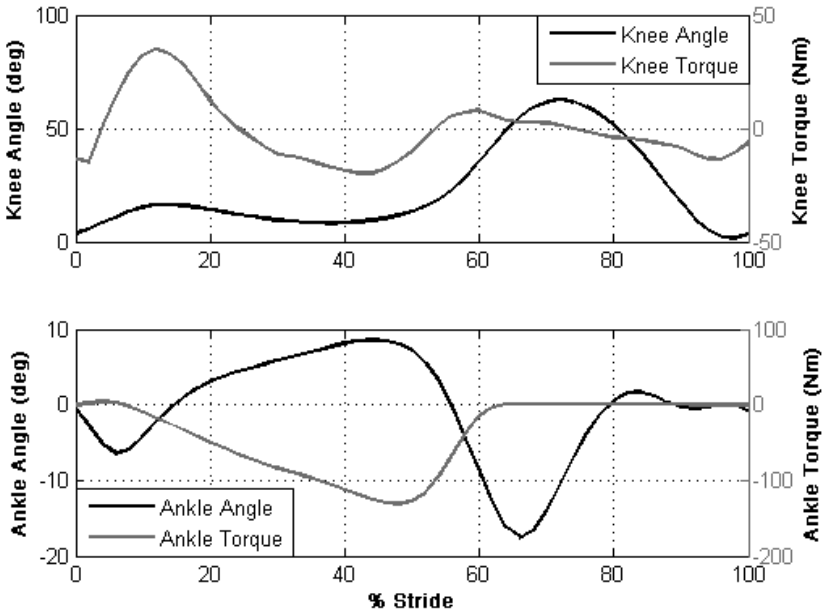

Figure 3-1. Normal biomechanical gait data for an 85 kg subject walking at a cadence of 80 steps per minute [9].

Table 3-1. Design specifications.

Specification	Value
Knee Range of Motion	0° to 120°
Ankle Range of Motion	-45° to 20°
Maximum Knee Torque	75 Nm
Maximum Ankle Torque	130 Nm
Peak Knee Power	150 W
Peak Ankle Power	250 W
Knee Center Height Adjustability	0.45 m to 0.58 m
Maximum Total Weight	4.5 kg
Minimum Factor of Safety	2

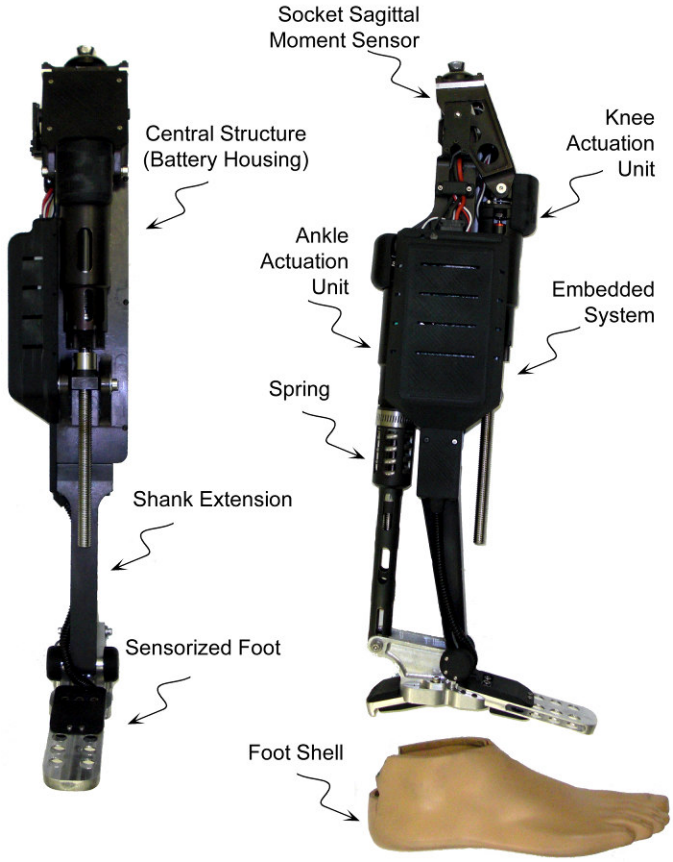

Figure 3-2. The self-contained powered knee and ankle transfemoral prosthesis, front (left) and side (right) views.

Mechanical Design

Actuation for the prosthesis is provided by two motor-driven ball screw assemblies that drive the knee and ankle joints, respectively, through a slider-crank linkage. The prosthesis is capable of 120° of flexion at the knee and 45° of planterflexion and 20° of dorsiflexion at the ankle. Each actuation unit consists of a Maxon EC30 Powermax brushless motor capable of producing 200 W of continuous power connected to a 12 mm diameter ball screw with 2 mm pitch, via helical shaft couplings. The ankle actuation unit additionally incorporates a 302 stainless steel spring (51mm free length and 35mm outer diameter), with 3 active coils and a stiffness of 385 N/cm in parallel with the ball screw. The purpose of the spring is to bias the motor's axial force output toward ankle plantarflexion, and to supplement power output during ankle push off. The stiffness of the spring is maximized to allow for peak force output without limiting the range of motion at the ankle. The resulting axial actuation unit's force versus ankle angle plot, Fig. 3-3, graphically demonstrates for fast walking the reduction in linear force output supplied by the motor at the ankle through the addition of the spring. Note that the compression spring does not engage until approximately five degrees of ankle plantarflexion. Each actuation unit additionally includes a uniaxial load cell (Measurement Specialties ELPF-500L), positioned in series with the actuation unit for closed loop force control of the motor/ballscrew unit. Both the knee and ankle joints incorporate bronze bearings and, for joint angle measurement, integrated precision potentiometers (ALPS RDC503013). A strain based sagittal plane moment sensor, Fig. 3-4, is located between the knee joint and the socket connector, which measures the moment between the socket and prosthesis. The ankle joint connects to a custom foot design, Fig. 3-5, which incorporates strain gages to measure the ground reaction forces on the ball of the foot and on the heel. The central hollow structure houses a lithium-polymer battery and provides an attachment point for the embedded system

hardware. To better fit with an anthropomorphic envelope, the ankle joint is placed slightly anterior to the centerline of the central structure. This gives the prosthesis the illusion of flexion when the amputee is standing vertically with the knee fully extended.

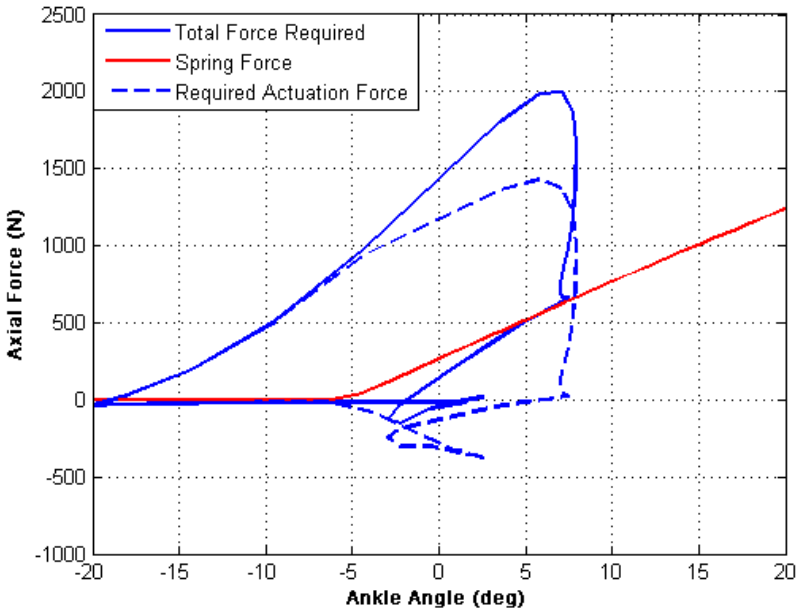

Figure 3-3. The reduction of linear force output required by the ankle motor unit by the addition of a spring in parallel for fast walking, taken from averaged normal biomechanical data [9].

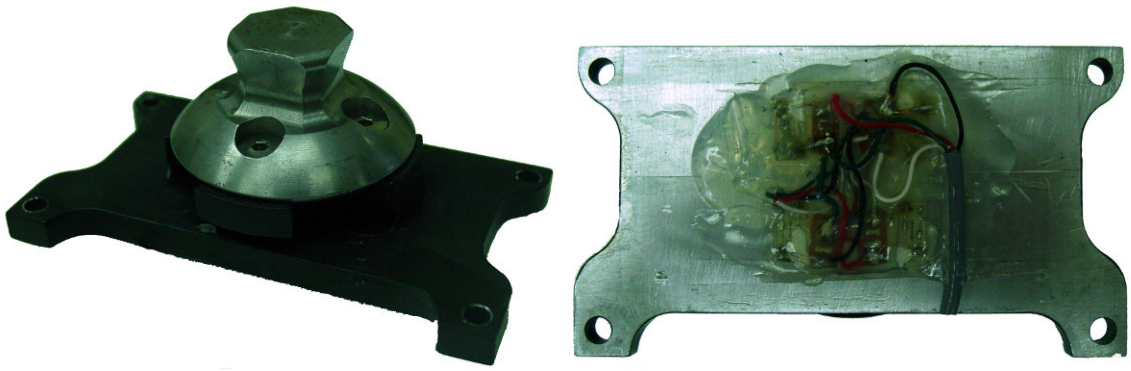

Figure 3-4. Sagittal moment load cell, top and bottom views.

Figure 3-5. Sensorized prosthetic foot with and without strain gage covers.

The length of the shank segment is varied by changing the length of three components; the lower shank extension, the spring pull-down, and the coupler between the ball nut and ankle. Additional adjustability is provided by the pyramid connector that is integrated into the sagittal moment load cell for coupling the prosthesis to the socket (as is standard in commercial transfemoral prostheses). The self-contained transfemoral prosthesis was fabricated from 7075 aluminum and has a total mass of 4.2 kg, which is within an acceptable range for transfemoral prostheses, and comparable to a normal limb segment [33]. A weight breakdown of the device is presented in Table 3-2.

Table 3-2. Mass breakdown of self-contained powered prosthesis.

Component	Mass (kg)
Battery	0.62
Electronics	0.36
Knee Motor Assembly	0.72
Ankle Motor Assembly	0.89
Sensorized Foot	0.35
Foot Shell	0.24
Sagittal Moment Sensor	0.12
Remaining Structure	0.90
Total Weight	4.20

Moment and Force Sensing

The sagittal plane moment between the user and prosthesis, and the force between the prosthesis and ground is sensed in order to infer user intent and coordinate prosthesis control. Based on biomechanical data [8, 9], the required range of measurements was determined to be 100 Nm of sagittal plane moment and a ground reaction force of 1000 N. The sagittal plane moment is measured above the knee joint at the socket interface and the ground reaction force is measured by the custom foot. The location of the sensors was chosen to avoid coupling the desired measured ground reaction force and sagittal moment with the joint torques. In addition, incorporating the ground reaction load cell into the structure of a custom foot eliminates the added weight of a separate load cell, and also enables separate measurement of the heel and ball of foot load.

The sagittal plane moment sensor, shown in Fig. 3-4, is designed to have a low profile in order to accommodate longer residual limbs. The sensor incorporates a full bridge of semiconductor strain gages which measure the strains generated by the sagittal plane moment. Finite element analysis, using ProEngineer Mechanica, was used to minimize the overall design height and to achieve the desired strains

in the load cell. The sensor is fabricated from 7075 aluminum and has an assembled weight of 120 grams including the stainless steel pyramid connector. The overall height of the sensor including the pyramid connector is 32 mm, with a rectangular base of 78 mm by 44 mm. The device was calibrated for a measurement range of 100 Nm, and exhibited linearity within ± 5% error over the full scale output.

The custom foot, shown in Fig. 3-5, was designed to measure the ground reaction force components at the ball of the foot and heel. The foot is comprised of heel and toe beams, rigidly attached to a central fixture and arranged as cantilever beams with an arch that allows for the load to be localized at the heel and ball of the foot, respectively. Each heel and toe beam incorporates a full bridge of semiconductor strain gages that measure the strains resulting from the respective ground contact forces. The foot utilized for the tests described herein measures 220 mm long, 56 mm wide and is 35 mm tall to the top of the central fixture and approximates a US size 12 or EU size 46 foot. The foot is fabricated from 7075 aluminum and weighs 350 grams. The dimensions and weight are similar to commercial low-profile carbon-fiber prosthetic feet, such as the Otto Bock Lo-Rider. The prosthetic foot was designed to be housed in a soft prosthetic foot shell, as shown in Fig. 3-2. The heel and ball of foot load sensors were calibrated for a measurement range of 1000 N, and demonstrated linearity within ± 4% error for the full scale output range.

Embedded System

The powered prosthesis contains an embedded microcontroller that allows for either tethered or untethered operation. The embedded system consists of signal processing, power supply, power electronics, communications and computation modules, Fig. 6. The system is powered by a lithium polymer battery with 29.6 V nominal rating and 4000 mA-hr capacity. The signal electronics require ±12 V and +3.3

V, which are provided via linear regulators to maintain low noise levels. For efficiency, the battery voltage is reduced by PWM switching amplifiers to ±15 V and +5 V prior to using the linear regulators. The power can be disconnected via a microcontroller that controls a solid state relay. The power status is indicated by LED status indicators controlled also by the microcontroller.

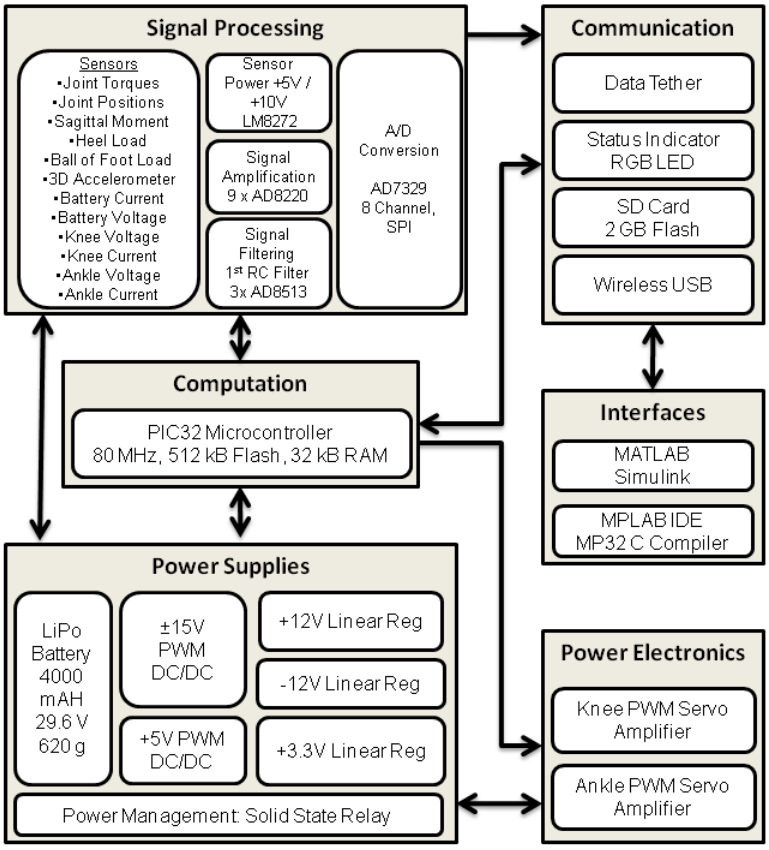

Figure 3-6. Embedded system framework.

The analog sensor signals acquired by the embedded system include the prosthesis sensors signals (five strain gage signals and two potentiometer signals), analog reference signals from the laptop computer used for tethered operation, and signals measured on the board including battery current and voltage, knee and ankle servo amplifier currents and a 3-axis accelerometer. The prosthesis sensor signals are conditioned

using input instrumentation amplifiers (AD8220) over a range of +/-10 V. The battery, knee motor and ankle motor currents are measured by current sensing across 0.02 Ohm resistors and via current sensing amplifiers (LT1787HV). The signals are filtered with a first-order RC filter with 1.6 kHz cut off frequency for the commercial load cells and joint angles and 160 Hz cutoff frequency for the sagittal moment, heel and ball of foot custom load cells and buffered with high slew rate amplifiers before the analog to digital conversion stage. Analog to digital conversion is accomplished by two 8-channel analog to digital convertors (AD7329). The analog to digital conversion data is transferred to the microcontroller via serial peripheral interface (SPI) bus.

The main computational element of the embedded system is an 80 MHz PIC32 microcontroller with 512 kB flash memory and 32 kB RAM, which consumes approximately 0.4 W of power. The microcontroller is programmed in C using MPLAB IDE and MP32 C Compiler. In addition to untethered operation, the prosthesis can also be controlled via a tether by a laptop computer running MATLAB Simulink RealTime Workshop. In the untethered operation state, the microcontroller performs the servo and activity controllers of the prosthesis and data logging at each sample time (1ms). In the tethered operation state, the microcontroller drives the servo amplifiers based on analog reference signals from the laptop computer. A 1 GB SD memory card is used for logging time-stamped data acquired from the sensors and recording internal controller information. The SD card is interfaced to the computer via wireless USB protocol. The microcontroller sends PWM reference signals to two four quadrant brushless DC motor drivers (Advanced Motion Control AZBDC20A8) rated at 12A continuous and 20A peak current output with regenerative capabilities in the second and forth quadrants of the velocity/torque curve.

The embedded system printed circuit board is a 130 mm x 90 mm 4-layer board designed for surface

mount technology (SMT) components. To further reduce the footprint of the board, the removable servo amplifiers were raised to allow for the placement of components underneath, as shown in Fig. 3-7. The mass of the embedded system is 0.36 kg, which consists of the board and components (0.10 kg), servo amplifiers (0.19 kg) and protective cover (0.07 kg).

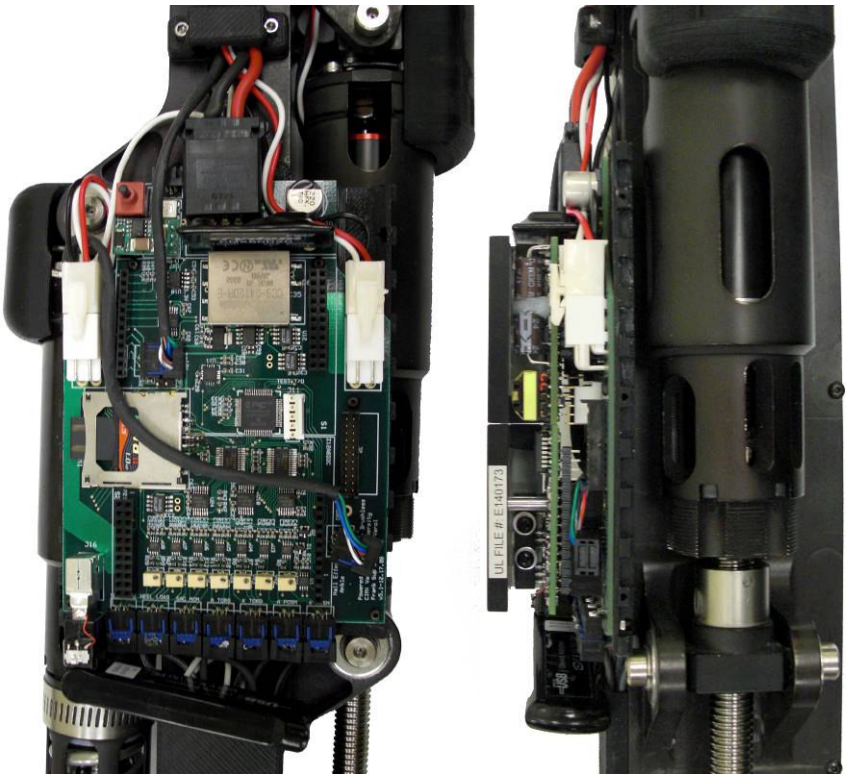

Figure 3-7. Embedded system hardware with (right) and without (left) servo amplifiers.

Control

The general control architecture of the prosthesis consists of three layers, as diagrammed in Fig. 3-8. The high-level supervisory controller, which is the intent recognizer, infers the user's intent based on the interaction between the user and the prosthesis, and switches the middle-layer controllers appropriately.

Intent recognition is achieved by first generating a database containing sensor data from different activity modes and training a pattern recognizer that switches between activity modes in real time, as described in [34]. A middle-layer controller is developed for each activity mode, such as walking, standing, sitting, and stair ascent/descent. The middle-layer controllers generate torque references for the joints using a finite state machine that modulates the impedance of the joints depending on the phase of the gait. The low-level controllers are the closed-loop joint torque controllers, which compensate for the transmission dynamics of the ball screw (i.e., primarily friction and inertia), and thus enable tracking of the knee and ankle joint torque references (commanded by the middle-layer controllers) with a higher bandwidth and accuracy than is afforded with an open-loop torque control approach.

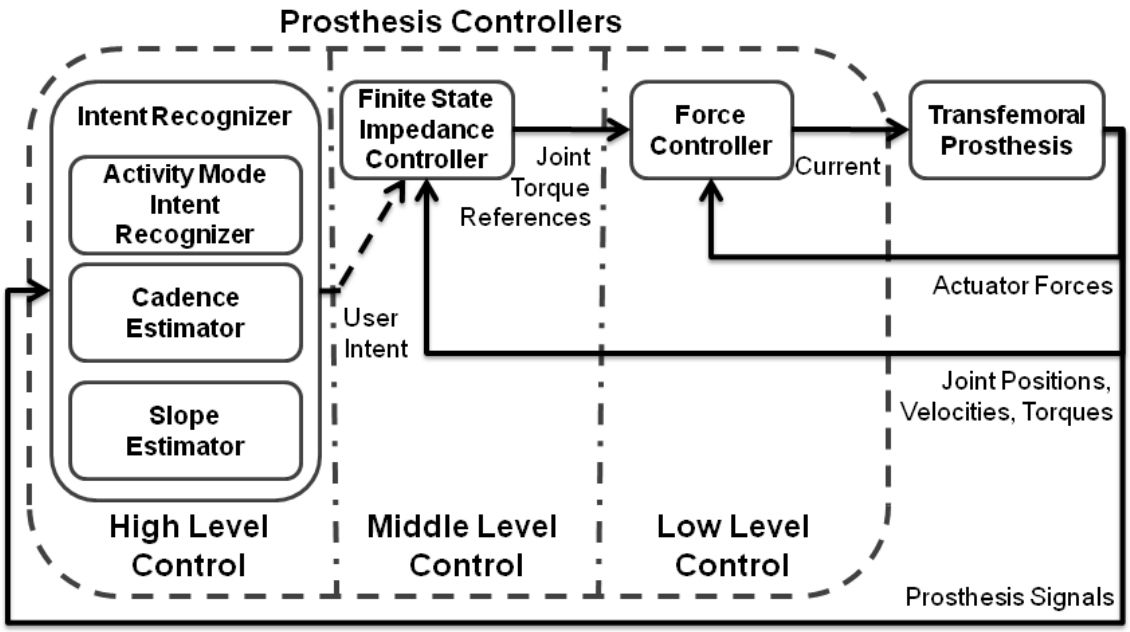

Figure 3-8. Complete control architecture showing high, middle and low levels.

The finite state impedance control developed by the authors utilizes an impedance-based approach to

generate joint torques [26]. The joint torques for each activity mode, such as walking, standing, sitting, stair ascent/descent, are governed by separate finite state machines, which modulate the joint impedance according to the phase of gait. The finite state machines for walking and standing are diagrammed in Figs. 3-9 and 3-10, respectively. The state model for walking is described by five phases, three of which are stance phases (early stance, middle stance, and late stance) and two of which are swing phases (swing knee flexion and swing knee extension). The standing state model is described by two phases, which are a weight bearing phase and a non-weight bearing phase. Note that the distinction between torque commands and position commands is largely one of output impedance. That is, accurate tracking of position trajectories requires a high joint output impedance, which is not characteristic of human gait. By generating torques trajectories rather than position trajectories, the output impedance of each joint can be more closely matched to the native limb, thus enabling the user to interact with the prosthesis by leveraging its dynamics in a manner similar to normal gait. In other words, the resulting motion of each prosthesis joint is due to the combination of the user input and the prosthesis input, rather than resulting from the prosthesis input alone (as would be the case with a position-based controller). In each phase, the knee and ankle torques, τ_i , are each described by a passive spring and damper with a fixed equilibrium point, given by:

$$\tau_i = k_i(\theta - \theta_{ki}) + b_i\dot{\theta} \tag{1}$$

where k_i , b_i , and θ_{ki} denote the linear stiffness, damping coefficient, and equilibrium point, respectively, for the i^{th} state. Energy is delivered to the user by switching between appropriate equilibrium points (of the virtual springs) during transitions between phases. In this manner, the prosthesis is guaranteed to be passive within each phase, and thus generates power simply by switching between phases. Since the user initiates phase switching, the result is a predictable controller that, barring phase switching input from the

user, will always default to passive behavior.

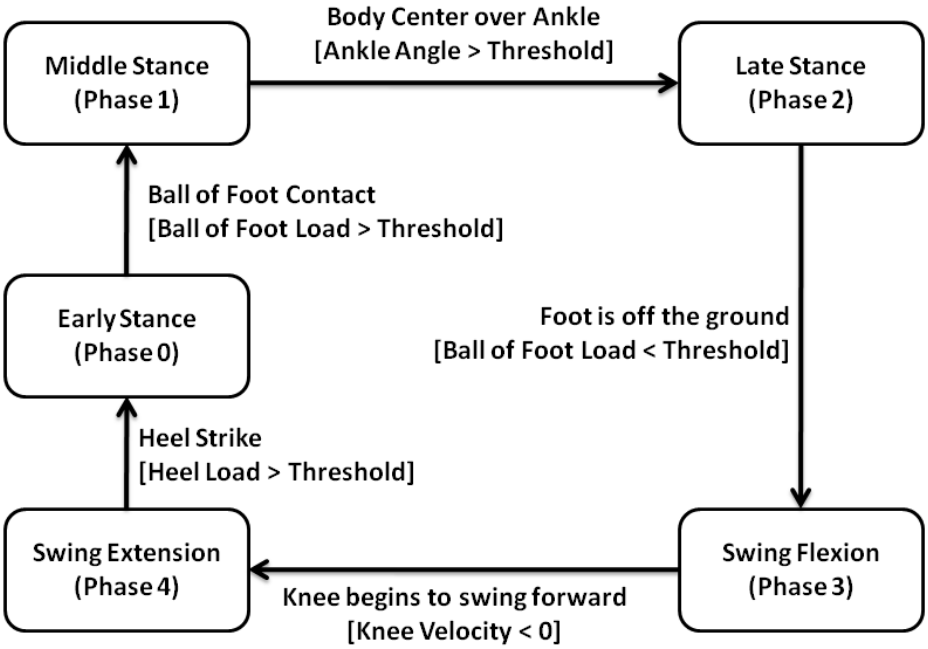

Figure 3-9. The finite state machine for level walking. Blocks represent states and arrows represent the corresponding transitions.

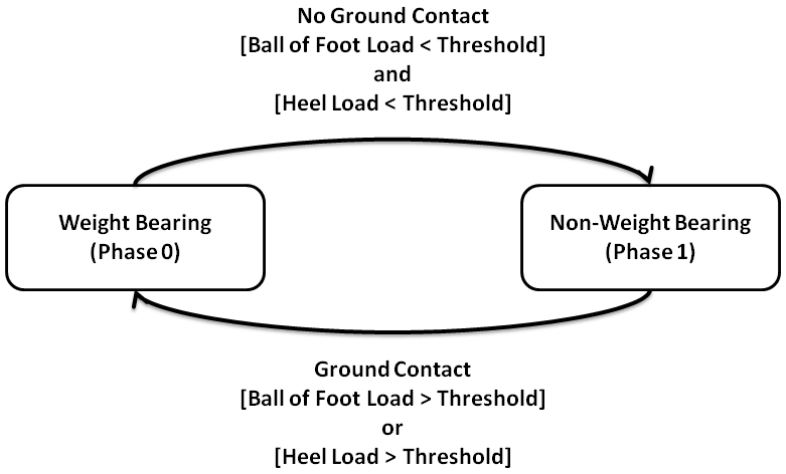

Figure 3-10. The finite state machine for level standing. Blocks represent states and arrows represent the corresponding transitions.

Experiments

The powered prosthesis was tested on a 20 year-old male (1.93 m, 75 kg) unilateral amputee three years post amputation. A photograph of the transfemoral amputee wearing the prosthesis is shown in Fig. 3-11. The length of the test subject's residual limb measured from the greater trochanter to the amputated site was 55% of the length of the non-impaired side measured from the greater trochanter to the lateral epicondyle. The subject uses an Otto Bock C-leg with a Freedom Renegade prosthetic foot for daily use. For testing of the powered prosthesis prototype, the subject's daily-use socket was used, with the height and varus-valgus alignment of the prosthesis adjusted for the initial trial by a licensed prosthetist.

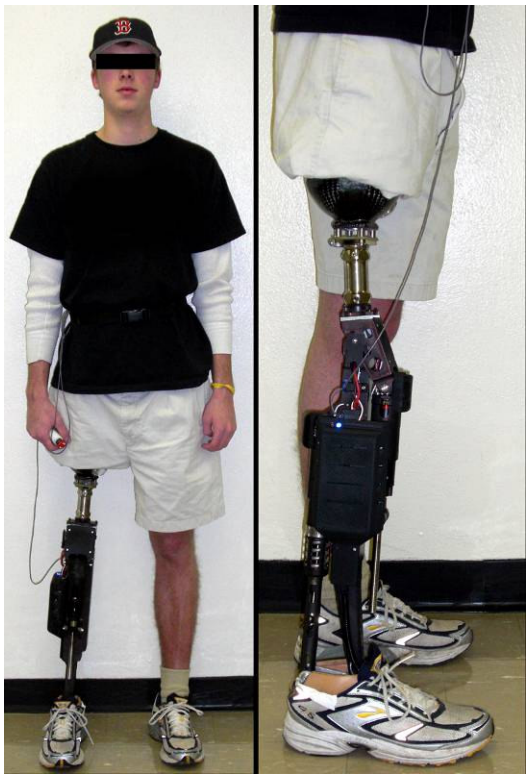

Figure 3-11. Unilaterial transfemoral amputee test subject used for the powered prosthesis evaluation.

Parameter Tuning

Experiments were performed to characterize the knee and ankle joint angles, torques, and power while walking over ground at a self-selected walking speed, and also to characterize the system's electrical power consumption, mechanical power generation, and efficiency. In order to conduct the over-ground characterization, a series of experiments were required to parameterize the middle-layer controller to the subject at various walking cadences. The controller parameterization was conducted on a treadmill at three walking cadences. The nominal cadence used for parameter tuning was the subject's self-selected cadence while wearing his daily-use prosthesis. For over-ground walking, the subject walked comfortably with his daily use (passive) prosthesis at 90 steps per minute at 4.1 km/h. For treadmill walking, the speed indicator on the treadmill was covered and the subject adjusted the treadmill speed until he felt comfortable. The self-selected normal cadence of the subject was determined to be 75 steps per minute at 2.8 km/h. Fast and slow cadences were set at ±15 percent of the normal treadmill cadence resulting in treadmill speeds of 2.2 and 3.4 km/h, respectively. The middle layer control parameters of the powered prosthesis were then tuned (with the prosthesis controlled in the tethered state) while walking on the treadmill at slow, normal and fast walking cadences (as determined by the daily use prosthesis), and also for standing. During the standing mode, the test subject alternately shifted his weight between limbs, turned in place, and stood still. Note that in all cases, the parameters were tuned using a combination of feedback from the user, and from visual inspection of the joint angle, torque, and power data. Note also that the tethered operating mode was utilized during treadmill parameter tuning because it enables quick and easy parameter variation and data visualization, and thus greatly expedites the iterative parameter tuning process. The resulting middle-layer controller parameters of the tuned impedance functions for standing and for the various

walking cadences are listed in Tables 3-3 and 3-4.

Table 3-3. Impedance parameters for treadmill walking from experimental tuning.

		Knee Impedance			Ankle Impedance		
Phas	Speed	k	b	θ_k	k	b	θ_k
	km h^{-1}	Nm deg^{-1}	N s m^{-1}	deg	Nm deg^{-1}	N s m^{-1}	deg
	2.2	2.5	0.05	8	3.0	0.04	-1
0	2.8	2.5	0.05	10	3.0	0.04	-1
	3.4	2.5	0.05	10	3.0	0.04	-1
	2.2	4.0	0.06	6	5.0	0.04	0
1	2.8	5.0	0.06	6	5.0	0.04	0
	3.4	5.0	0.06	6	5.0	0.04	0
	2.2	3.0	0.02	14	4.0	0.01	-16
2	2.8	3.5	0.02	14	5.0	0.01	-16
	3.4	5.0	0.02	14	5.0	0.01	-16
	2.2	0.15	0.02	65	0.4	0.05	0
3	2.8	0.10	0.02	65	0.4	0.05	0
	3.4	0.10	0.01	65	0.4	0.05	0
	2.2	0.10	0.03	40	0.7	0.03	0
4	2.8	0.20	0.03	40	0.7	0.03	0
	3.4	0.25	0.03	40	0.7	0.03	0

Note: Highlighted parameters vary with walking speed.

Table 3-4. Impedance parameters for standing from experimental tuning.

	Knee Impedance			Ankle Impedance		
Phase	k	b	θ_k	k	b	θ_k
	Nm deg^{-1}	N s m^{-1}	deg	Nm deg^{-1}	N s m^{-1}	deg
0	2.5	0.02	0	4.0	0.05	-6
1	0	0.02	0	2.0	0.05	-6

The measured joint angles from the prosthesis' on-board sensors during level treadmill walking at cadences of 64, 75 and 87 steps per minute are shown in Fig. 3-12. In comparing the knee and ankle angles

to prototypical data from normal subject, Fig. 3-1, one can observe that the powered prosthesis and controller provide knee and ankle joint angle profiles quite similar to those observed during normal gait. The ability of the device to provide stance flexion provides cushioning at heel strike and reduces the rise of the body's center of mass to allow for more efficient gait [35].

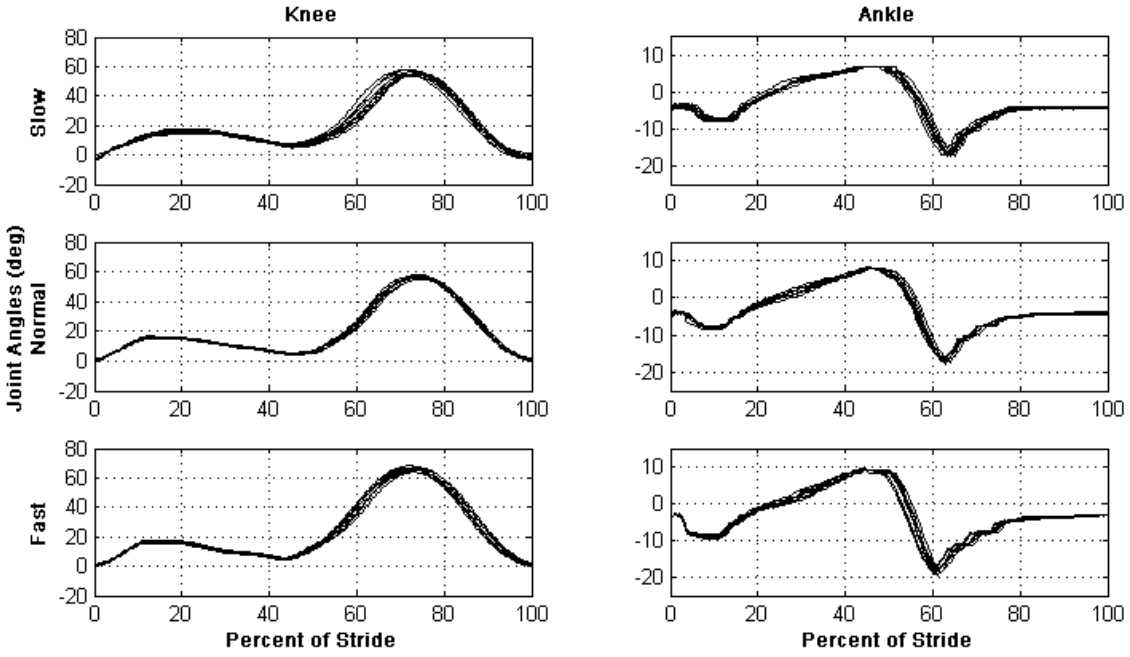

Figure 3-12. Measured joint angles of the powered prosthesis for ten consecutive gait cycles of treadmill walking at slow, normal and fast cadences, 64, 75, and 86 steps per minute, respectively.

Over-ground Walking

Once the middle-layer controllers were fully parameterized for standing and slow, medium (i.e., self-selected), and fast cadences, the prosthesis was switched to the untethered operating mode, so that the subject could walk over-ground with the fully self-contained prosthesis (i.e., without a tether hindering movement). The subject walked on a straight, 50 m track (actually a hallway) at a self-selected cadence. The best walking performance was achieved using the fast (87 steps per minute) impedance controller. As

has been documented by others (e.g., see [36]), the mechanics of treadmill walking are not entirely consistent with the dynamics of over-ground walking, and as such the self-selected speeds over-ground are typically significantly faster than self-selected speeds on a treadmill. Consistent with this phenomenon, the subject's self-selected speed during the over-ground walking tests was 87 steps per minute, which corresponded to a walking speed of 5.1 km/h, both of which are significantly greater than the self-selected treadmill walking (which were 75 steps per minute and 2.8 km/h, respectively). Furthermore, the subject's over-ground self-selected speed increased 24 percent from 4.1 km/h to 5.1 km/h while using the powered prosthesis. The subject walked on the 50 m track at a self-selected speed for a total of 10 trials while prosthesis data (i.e., servo amplifier currents, battery current and voltage, joint positions, velocities and torques, socket sagittal plane moment, heel and ball of foot loads, three dimensional shank accelerations, and controller state information) were collected at a 200 Hz sampling rate.

Measured joint angles, torques and powers from walking on level ground at the self-selected cadence for ten consecutive strides are shown in Fig. 3-13. As indicated by the data, the powered prosthesis provides knee torques over 40 Nm (during stance flexion) and ankle torques approaching 120 Nm during toe-off. As shown in the power data, the prosthesis is contributing significant positive power (during stance) at both the knee joint (peak powers of 50 W) and ankle joint (peak powers approaching 250 W). For each stride, the prosthesis delivers 13.8 J of net energy on average at the ankle. Finally, the torque tracking for the knee and ankle joints, shown in Fig. 3-14, indicates good torque tracking, and further indicates that the torque and power capabilities of the self-powered prosthesis are well-suited to the demands of the controller.

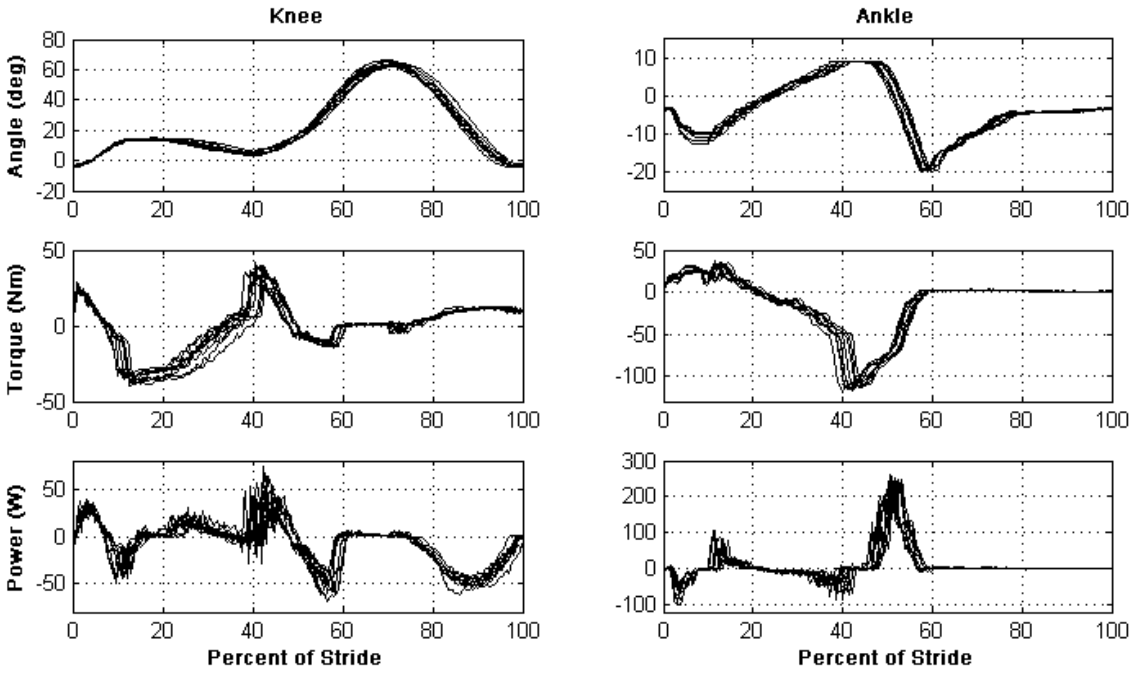

Fig. 3-13. Measured joint angles, torques and powers of the powered prosthesis for ten consecutive gait cycles at self-selected speed (5.1 km/h at 87 steps per minute).

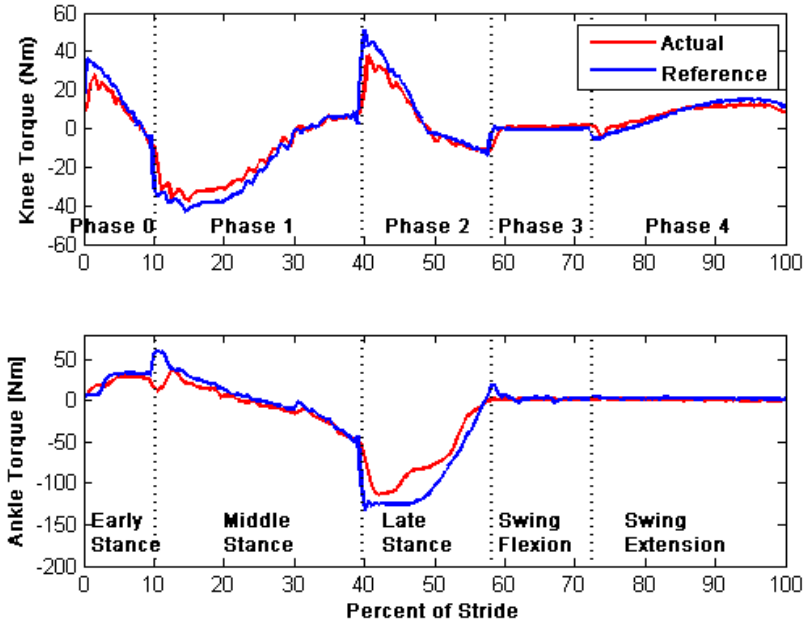

Figure 3-14. References and actual knee and ankle joint torques of the powered prosthesis for one stride at self-selected speed (5.1 km/hr at 87 steps per minute) on normal ground.

Power Consumption and Battery Life

One of the primary constraints of the electrically powered knee and ankle prosthesis design is the power source. As such, the electrical power consumption was measured to characterize the potential battery life and range of the device. The electrical power consumed (at the motor leads) and the mechanical power generated over one gait cycle are shown in Fig. 3-15. Electrical power regeneration (afforded by the regenerative servo amplifiers) is observed in the late swing gait phase in the knee. It is interesting to note that the peak electrical power event for level walking at the knee joint occurs at heel strike. At the ankle joint, a peak mechanical power output of over 200W is experienced at toe-off, which requires approximately 50 percent more electrical power at the motor leads.

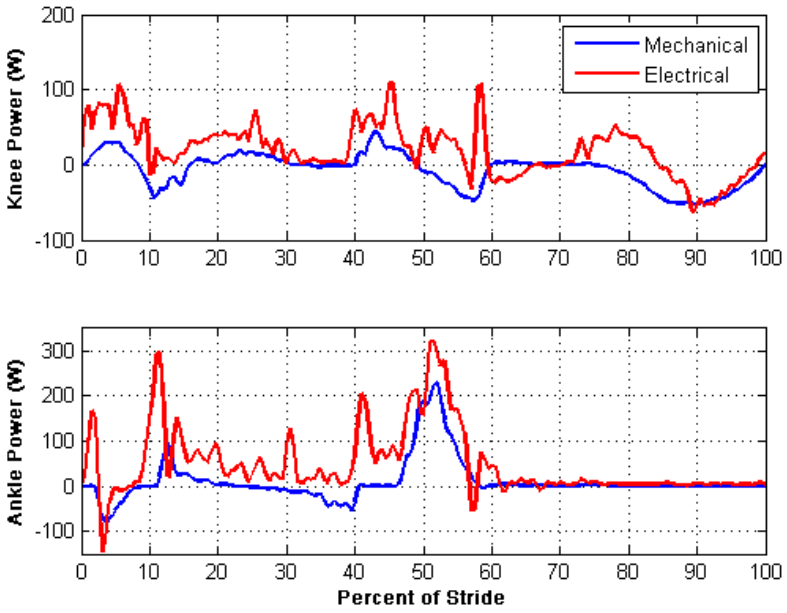

Figure 3-15. Measured electrical and mechanical power at the knee and ankle joints of the powered prosthesis over one gait cycle at self-selected speed (5.1 km/hr at 87 steps per minute) on normal ground.

In order to characterize battery requirements, the average electrical power required by prosthesis (i.e., the embedded system, knee joint, and ankle joint) during standing and walking over level ground (at the self-selected speed of 5.1 km/h) is shown in Fig. 3-16. The total average power consumption for level ground walking and standing is 66 W and 10 W, respectively. Since the prosthesis incorporates a (rechargeable) 118 Watt-hr lithium polymer battery, such electrical power requirements suggest a battery life between charges of approximately 1.8 hours of walking or 12 hours of standing. With these figures, the prosthesis is capable of over 4,500 strides (9,000 steps by the user) with the prosthesis at the self-selected cadence. Given the walking speed of 5.1 km/h, the measured power requirements indicate a walking distance (for the amputee subject) of 9.0 km. Note that if the energy density of lithium ion battery technology doubles over the next five years (as is projected [31]), the walking range between battery charges would similarly double approaching 20 km.

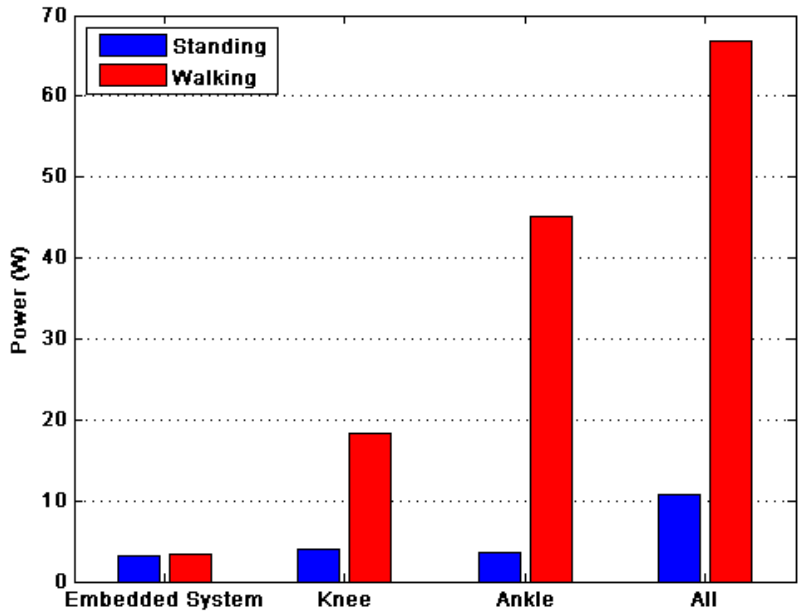

Figure 3-16. Average electrical power consumption of the powered prosthesis for standing and walking at self-selected speed (5.1 km/hr at 87 steps per minute) on normal ground.

Conclusion

The paper describes the design and control of a fully self-contained electrically powered knee and ankle prosthesis capable of producing human-scale power. Experimental results with a unilateral amputee indicate that the device can provide transfemoral amputee biomechanics during walking similar to those typically observed during healthy biomechanics. Power consumption measurements on level ground indicate that device consumes 66 W at a walking speed of 5.1 km/h on a 75 kg subject. As such, given the specifications of the on-board battery pack, the prosthesis can provide 9.0 km of level, over-ground walking between recharges. Future works include addressing the audible noise of the device and a comprehensive biomechanical evaluation of the powered prosthesis on multiple amputee subjects.

References

[1] P. F. Adams, G. E. Hendershot, and M. A. Marano, “Current estimates from the National Health Interview Survey, 1996,” *National Center for Health Statistics. Vital Health Stat 10(200)*, 1999.

[2] J. Feinglass, J. L. Brown, A. LaSasso, M. W. Sohn, L. M. Manheim, S. J. Shah, and W. H. Pearce, “Rates of lower-extremity amputation and arterial reconstruction in the United States, 1979 to 1996,” *American J. of Public Health,* vol. 89, no. 8, pp. 1222-1227, Aug, 1999.

[3] P. DeVita, M. Torry, K. L. Glover, and D. L. Speroni, “A functional knee brace alters joint torque and power patterns during walking and running,” *J. of Biomechanics,* vol. 29, no. 5, pp. 583-588, May, 1996.

[4] R. Jacobs, M. F. Bobbert, and G. J. van Ingen Schenau, “Mechanical output from individual muscles during explosive leg extensions: The role of biarticular muscles,” *J. of Biomechanics,* vol. 29, no. 4, pp. 513-523, Apr, 1996.

[5] S. Nadeau, B. J. McFadyen, and F. Malouin, “Frontal and sagittal plane analyses of the stair climbing task in healthy adults aged over 40 years: what are the challenges compared to level walking?,” *Clinical Biomechanics,* vol. 18, no. 10, pp. 950-959, Dec, 2003.

[6] A. Nagano, Y. Ishige, and S. Fukashiro, “Comparison of new approaches to estimate mechanical output of individual joints in vertical jumps,” *J. of Biomechanics,* vol. 31, no. 10, pp. 951-955, Oct, 1998.

[7] B. I. Prilutsky, L. N. Petrova, and L. M. Raitsin, “Comparison of mechanical energy expenditure of joint moments and muscle forces during human locomotion,” *J. of Biomechanics,* vol. 29, no. 4, pp. 405-415, Apr, 1996.

[8] R. Riener, M. Rabuffetti, and C. Frigo, “Joint powers in stair climbing at different slopes,” *Proc. of the First Joint BMES/EMBS Conf.,* vol. 1, pp. 530 vol.1, 1999.

[9] D. Winter, *The Biomechanics and Motor Control of Human Gait: Normal, Elderly and Pathological*, 2nd ed.: University of Waterloo Press, 1991.

[10] D. A. Winter, and S. E. Sienko, “Biomechanics of below-knee amputee gait,” *J. of Biomechanics,* vol. 21, no. 5, pp. 361-367, 1988.

[11] R. L. Waters, J. Perry, D. Antonelli, and H. Hislop, “Energy cost of walking of amputees - Influence of level of amputation,” *J. of Bone and Joint Surgery-American Vol.,* vol. 58, no. 1, pp. 42-46, 1976.

[12] M. Donath, “Proportional EMG control for above knee prostheses,” Massachusetts Institute of Tech. Dept. of Mechanical Eng. Thesis. M.S., 1974.

[13] W. C. Flowers, “A man-interactive simulator system for above-knee prosthetics studies,” Massachusetts Institute of Tech. Dept. of Mechanical Eng. Thesis. Ph.D., 1973.

[14] W. C. Flowers, and R. W. Mann, “Electrohydraulic knee-torque controller for a prosthesis simulator,” *ASME J. of Biomechanical Engineering,* vol. 99, no. 4, pp. 3-8, 1977.

[15] D. L. Grimes, “An active multi-mode above knee prosthesis controller,” Massachusetts Institute of Tech. Dept. of Mechanical Eng. Thesis Ph.D., 1979.

[16] D. L. Grimes, W. C. Flowers, and M. Donath, “Feasibility of an active control scheme for above knee prostheses,” *ASME J. of Biomechanical Engineering,* vol. 99, no. 4, pp. 215-221, 1977.

[17] J. L. Stein, and W. C. Flowers, “Stance phase-control of above-knee prostheses - Knee control versus SACH foot design,” *J. of Biomechanics,* vol. 20, no. 1, pp. 19-28, 1987.

[18] J. L. Stein, and Massachusetts Institute of Technology. Dept. of Mechanical Engineering., “Design issues in the stance phase control of above-knee prostheses,” Massachusetts Institute of Tech. Dept. of Mechanical Eng. Thesis Ph.D., 1983.

[19] D. Popovic, and L. Schwirtlich, “Belgrade active A/K prosthesis,” *in de Vries, J. (Ed.), Electrophysiological Kinesiology, Intern. Congress Ser. No. 804, Excerpta Medica, Amsterdam, The Netherlands*, pp. 337-343, 1988.

[20] S. Bedard, and P. Roy, *Actuated leg prosthesis for above-knee amputees*, 7,314,490, U. S. Patent, June 17, 2003.

[21] E. Martinez- Villalpando, J. Weber, G. Elliott, and H. Herr, “Design of an agonist-antagonist active knee prosthesis,” *Proc. IEEE/RAS-EMBS Int. Conf. on Biomedical Robotics and Biomechatronics*, pp. 529-534, 2008.

[22] G. K. Klute, J. Czerniecki, and B. Hannaford, “Muscle-like pneumatic actuators for below-knee prostheses,” *Proc. 7th Int. Conf. on New Actuators*, pp. 289-292, 2000.

[23] W. Koniuk, *Self-adusting prosthetic ankle apparatus*, 6,443,993, U. S. Patent, March, 23, 2001.

[24] R. Bellman, A. Holgate, and T. Sugar, “SPARKy 3: Design of an active robotic ankle prosthesis with two actuated degrees of freedom using regenerative kinetics,” *Proc. IEEE/RAS-EMBS Int. Conf. on Biomedical Robotics and Biomechatronics*, pp. 511-516, 2008.

[25] S. Au, and H. Herr, “Powered ankle-foot prosthesis,” *IEEE Robotics & Automation Magazine,* vol. 15, pp. 52-59, 2008.

[26] F. Sup, A. Bohara, and M. Goldfarb, “Design and control of a powered transfemoral prosthesis,” *Int. J. of Robotics Research,* vol. 27, no. 2, pp. 263-273, Feb, 2008.

[27] K. B. Fite, and M. Goldfarb, “Design and energetic characterization of a proportional-injector monopropellant-powered actuator,” *IEEE/ASME Trans. on Mechatronics,* vol. 11, no. 2, pp. 196-204, Apr, 2006.

[28] K. B. Fite, J. E. Mitchell, E. J. Barth, and M. Goldfarb, “A unified force controller for a proportional-injector direct-injection monopropellant-powered actuator,” *J. of Dynamic Systems Measurement and Control Trans. of ASME,* vol. 128, no. 1, pp. 159-164, Mar, 2006.

[29] M. Goldfarb, E. J. Barth, M. A. Gogola, and J. A. Wehrmeyer, “Design and energetic characterization of a liquid-propellant-powered actuator for self-powered robots,” *IEEE/ASME Trans. on Mechatronics,* vol. 8, no. 2, pp. 254-262, 2003.

[30] B. L. Shields, K. B. Fite, and M. Goldfarb, “Design, control, and energetic characterization of a solenoid-injected monopropellant-powered actuator,” *IEEE/ASME Trans. on Mechatronics,* vol. 11, no. 4, pp. 477-487, Aug, 2006.

[31] “In search of the perfect battery,” *Economist,* vol. 386, no. 8570, pp. 22-24, 2008.

[32] F. Sup, H. A. Varol, J. Mitchell, T. Withrow, and M. Goldfarb, “Design and control of an active electrical knee and ankle prosthesis,” *Proc. IEEE/RAS-EMBS Int. Conf. on Biomedical Robotics and Biomechatronics*, pp. 523-528, 2008.

[33] C. E. Clauser, J. T. McConville, and J. M. Young, “Weight, volume and center of mass of segments of the human body,” *AMRL-TR-69-70, Wright Patterson Airforce Base, Dayton, Ohio*, 1969.

[34] H. A. Varol, F. Sup, and M. Goldfarb, “Real-time gait mode intent recognition of a powered knee and ankle prosthesis for standing and walking,” *Proc. IEEE/RAS-EMBS Int. Conf. on Biomedical Robotics and Biomechatronics*, pp. 66-72, 2008.

[35] S. Blumentritt, H. Scherer, U. Wellershaus, and J. Michael, “Design principles, biomechanical data and clinical experience with a polycentric knee offering controlled stance phase knee flexion: A preliminary report,” *J. of Prosthetics and Orthotics,* vol. 9, no. 1, pp. 18-24, 1997.

[36] M. Traballesi, P. Porcacchia, T. Averna, and S. Brunelli, “Energy cost of walking measurements in subjects with lower limb amputations: A comparison study between floor and treadmill test,” *Gait & Posture,* vol. 27, no. 1, pp. 70-75, Jan, 2008.

CHAPTER IV

Manuscript 3: Powered Sit-to-Stand and Assistive Stand-to-Sit Framework For a Powered Transfemoral Prosthesis

Huseyin Atakan Varol, Frank Sup and Michael Goldfarb

Vanderbilt University

Nashville, TN 37235

Accepted as a Technical Paper to the

2009 IEEE International Conference on Rehabilitation Robotics

Abstract

This work extends the three level powered knee and ankle prosthesis control framework previously developed by the authors by adding sitting mode. A middle level finite state based impedance controller is designed to accommodate sitting, sit-to-stand and stand-to-sit transitions. Moreover, a high level Gaussian Mixture Model based intent recognizer is developed to distinguish between standing and sitting modes and switch the middle level controllers accordingly. Experimental results with unilateral transfemoral amputee subject show that sitting down and standing up intent can be inferred from the prosthesis sensor signals by the intent recognizer. Furthermore, it is demonstrated that the prosthesis generates net active power of 50 W during standing up and dissipates up to 50 W of power during stand-to-sit transition at the knee joint.

Introduction

Standing up is a frequently exercised daily activity which involves the coordinated movement of the entire body to substantially raise the body center of mass in a generally economical manner. It requires significant torque and range of motion at the knee joint and to a lesser extent the ankle joint [1-5]. Fundamentally, the ability to stand up from a seated position is a prerequisite to begin walking and extend one's mobility. In general, transfemoral amputees with prostheses that lack active power can have difficulty standing up or are unable to without aid, thus, predisposing them to a sedentary lifestyle. For a transfemoral amputee to accomplish the sit-to-stand transition unaided, requires twice the torque output from the sound side knee joint as compared to heFaalthy subjects [6] and additionally requires significantly increased compensatory torques in the frontal plane. Furthermore, the amputee does not bear weight on the prosthesis until they are

almost in the standing position [6]. To compensate for the lack of power in the lower limb, amputees often rely on the aid of their upper limbs and handrails. Conversely, passive prostheses are more assistive while sitting down. They enable the user to bear weight on both sides reducing excessive torques on the sound side joint. State-of-the-art microcontroller modulated braking knees adjust the damping on the knee joint to control the resistance during stand to sit transition [7]. However, an active prosthesis would benefit the user during stand-to-sit transition by providing active power to recover to the standing position in case the user changes his or her intent to sit down. The quality of life and mobility of transfemoral amputees could benefit from active assistance provided by a prosthesis with powered joints during the standing up (SU) and sitting down (SD) transitions.

The design of powered transfemoral prostheses is a challenging task due to the large range of motion on the knee joint and the magnitude of the power and torques that need to be applied at both the knee and ankle. Development of powered transfemoral prostheses dates back to the early 1970's with a tethered electro-hydraulically actuated knee joint. This prosthesis was a test bed for studying the feasibility of powered knee joints during walking [8]. Other prior work was conducted on the development of an active knee joint actuated by electrical motors with finite state position controller [9]. Ossur, a prosthetics company, introduced a powered knee prosthesis that is capable of generating net active power [10]. An agonist-antagonist knee design which utilizes the passive dynamics of the knee during walking is presented in [11]. The authors were not able to find any scientific literature on SU and SD transitions for these active transfemoral prostheses.

A self-contained powered knee and ankle prosthesis has been developed by the authors which aims to restore normal locomotive function to transfemoral amputees. The authors have also explored a three level

control architecture consisting of a high level intent recognizer, a middle level finite state based impedance controller and low level force-controller for walking and standing. In this work, the control architecture will be expanded to include sitting and the associated SU and SD transitions. The paper is designed as follows. Firstly, the powered prosthesis used in this study is presented. Secondly, the finite state based impedance controller for standing, sitting, and SU and SD transitions is described. Thirdly, the design of the intent recognizer for the sitting mode is described. Finally, experimental results with a unilateral transfemoral amputee are presented and discussed.

Methodology

Powered Prosthesis

The authors have previously described a tethered powered knee and ankle prosthesis [12]. A new (previously unreported) self-contained version of the prosthesis, shown in Fig. 4-1, was used for the powered sit-to-stand and assistive stand-to-sit testing, described herein. The powered prosthesis is a two degree of freedom robotic device capable of generating human-scale torque and power at the knee and ankle joints. Actuation of each joint is accomplished via slider-crank linkages driven by motor ball screw assemblies. The ankle actuation unit incorporates a spring to bias the motor's axial force output toward ankle plantarflexion, and to supplement power output during ankle push off. The device's sensor package includes a custom load cell to measure the sagittal socket interface moment above the knee joint, a custom foot to measure the ground reaction force at the heel and ball of the foot, and commercial potentiometers and load cells to measure joint positions and torques, respectively. The self-contained version hosts an embedded system allowing for both tethered and untethered operation run by either MATLAB Simulink or a

PIC32 microcontroller, respectively. The prosthesis is powered by a 118 W·h lithium polymer battery that allows for approximately 1.8 hours of level ground walking at 5.1 km/h (over 4,500 strides with the prosthesis) or 12 hours of standing, estimated in initial trials with one unilateral transfemoral amputee subject.

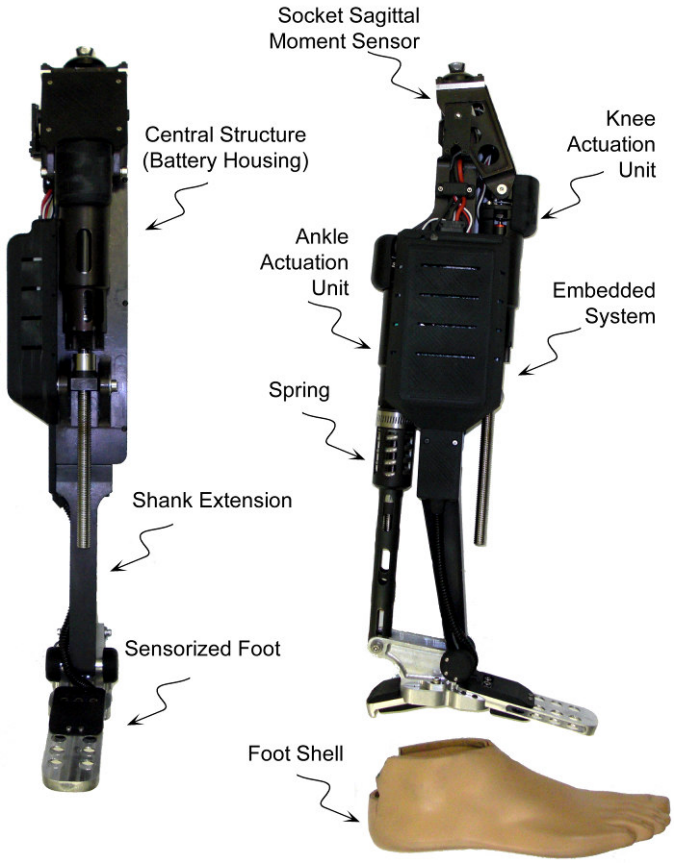

Figure 4-1. The self-contained powered knee and ankle transfemoral prosthesis.

Control Architecture

The control architecture of the prosthesis is a three level hierarchy, as diagrammed in Fig. 4-2. The high level supervisory controller, which is the intent recognizer, infers the user's intent based on the interaction between the user and the prosthesis, and correspondingly switches the middle level controllers. Intent

recognition is achieved by first generating a database containing sensor data from different activity modes and then training a pattern recognizer that switches between activity modes in real time, as described in [13]. A middle level controller is developed for each activity mode, such as walking, standing, sitting, and stair ascent/descent. The middle level controllers generate torque references for the joints using a finite state machine that modulates the impedance of the joints depending on the phase of the activity. The low-level controllers are the closed-loop joint torque controllers, which compensate for the transmission dynamics of the ball screw (i.e., primarily friction and inertia), and thus enable tracking of the knee and ankle joint torque references (commanded by the middle level controllers) with a higher bandwidth and accuracy than is afforded with an open-loop torque control approach. In this work, the design of the supervisory intent recognizer and the finite state impedance based controller for the sitting and standing modes will be presented.

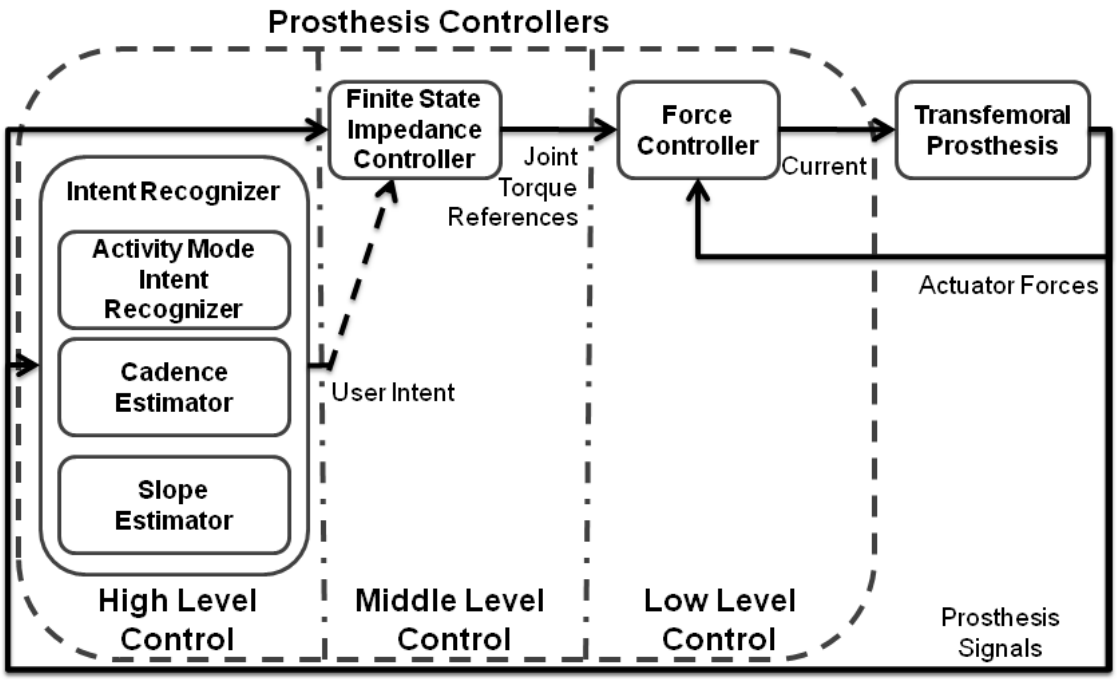

Figure 4-2. Powered prosthesis control architecture.

Finite State Based Impedance Control

In the finite state impedance based control, the impedance behavior of healthy biomechanical gait is mimicked by modulating joint impedances of the prosthesis according to the phase of gait. In each phase, the knee and ankle torques, τ_i, are each described by a passive spring and damper with a fixed equilibrium point, given by:

$$\tau_i = k_i(\theta - \theta_{ki}) + b_i\dot{\theta} \qquad (1)$$

where k_i, b_i, and θ_{ki} denote the linear stiffness, damping coefficient, and equilibrium point, respectively, for the i^{th} state. Switching joint impedances between the gait phases is initiated by biomechanical cues. For instance, the switching from swing extension to the early stance state during walking occurs with the detection of heel strike. The approach requires the development of a state machine for each type of user activity such as walking, standing, sitting, and stair ascent and descent. The result is an effective and

predictable controller that does not violate passive behavior except when the user requests active power transfer by triggering a transition. The authors previously developed controllers for standing and walking modes using this framework [12]. Within this framework, the finite state based impedance control approach will be extended to include a state machine for sitting and the transitions between sitting and standing, Fig. 4-3.

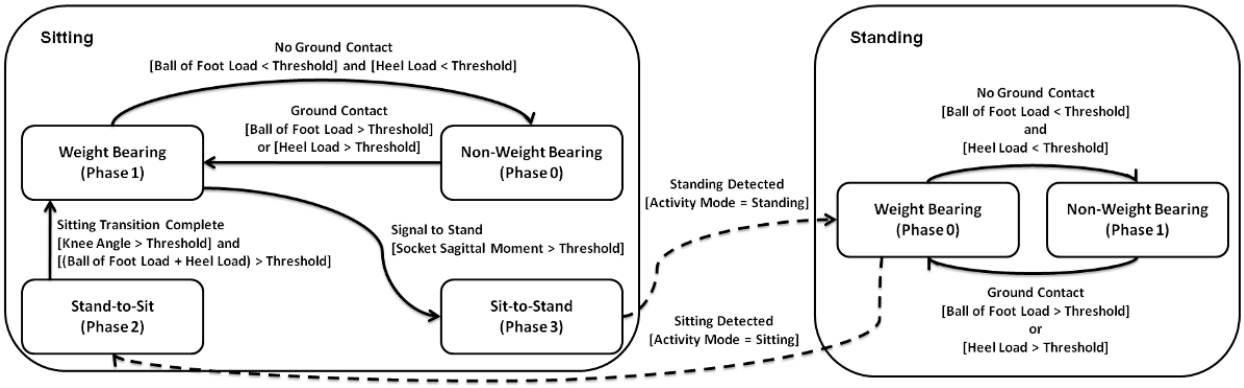

Figure 4-3. The state chart depicting the phase transitions in standing and sitting modes.

The standing impedance controller consists of two phases: weight bearing and non-weight bearing. In the weight bearing phase, the weight of the user is supported with high impedance at the joints. In the non-weight bearing mode, the knee acts as a soft dashpot to enable freedom of movement and a smooth transition to walking. While using the standing controller, the user can shift his or her weight between the sound side and the prosthesis, balance and shuffle. The sitting mode controller consists of four phases. Two are primary sitting phases, weight bearing and non-weight bearing. The other two encompass the transition phases, sit-to-stand and stand-to-sit transitions, for SU and SD, respectively. Weight bearing and non-weight bearing are the active sitting phases that switch the knee and ankle joints between high and low

impedances, respectively. The transition phases, sit-to-stand and stand-to-sit, modulate the stiffness of the knee as a function of knee angle, Fig. 4, to assist the user in SU and SD. The modulation allows for smoother transitions near the seated position. The ankle joint is slightly dorsiflexed with moderate stiffness during the SU and SD phases. The parameters of the impedance based controllers are tuned using a combination of feedback from the user and joint angle, torque and power data from the prosthesis.

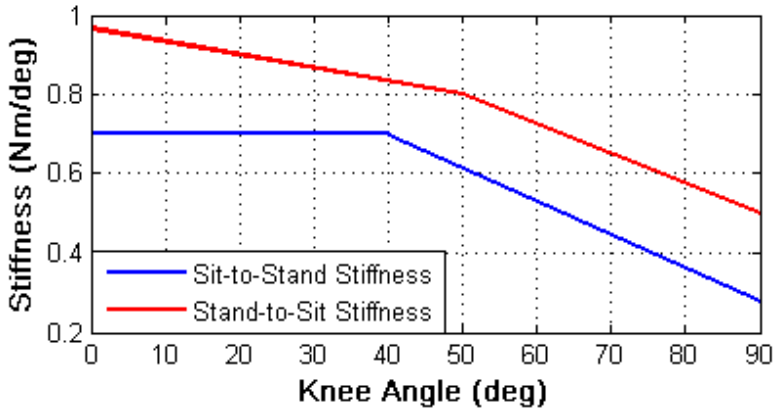

Figure 4-4. Knee angle modulated knee stiffness during sit-to-stand and stand-to-sit phases.

Intent Recognition

Database Generation

The prosthesis was tested on a 20-year-old male (1.93 m, 70 kg) unilateral amputee three years post amputation. The length of the test subject's residual limb, measured from the greater trochanter to the amputated site, was 55% of the length of the non-impaired side measured from the greater trochanter to the lateral epicondyle. The subject uses an Ottobock C-leg with a Freedom Renegade prosthetic foot for daily use. The subject's daily use socket was used on all experiments, where the powered prosthesis prototype was attached on place of the daily use prosthesis. The overall prosthesis height and varus-valgus alignment were performed by a licensed prosthetist. The prosthesis was tuned for the subject. The controller

parameters for the standing and sitting mode are given in Table 4-1 and 4-2, respectively, which were obtained by tuning as previously mentioned. The powered prosthesis was tethered to a laptop computer running MATLAB Real Time Workshop for controller implementation and data logging. The prosthesis sensor data for database generation was sampled at 1000 Hz consisted of seven signals: joint positions and velocities for the knee and ankle, socket sagittal plane moment and heel and ball of foot forces.

Table 4-1. Impedance parameters for standing from experimental tuning.

	Knee Impedance			Ankle Impedance		
Phase	k Nm deg^{-1}	b N s m^{-1}	θ_k deg	k Nm deg^{-1}	b N s m^{-1}	θ_k deg
0	2.5	0.02	0	4.0	0.05	-6
1	0	0.02	0	2.0	0.05	-6

Table 4-2. Impedance parameters for sitting from experimental tuning.

	Knee Impedance			Ankle Impedance		
Phase	k Nm deg^{-1}	b N s m^{-1}	θ_k deg	k Nm deg^{-1}	b N s m^{-1}	θ_k deg
0	0	0.05	0	4	0.06	0
1	0	0.02	0	2	0.02	0
2	1.0	0	5	2	0.06	5
3	0.7	0	5	2	0.06	5

In order to recognize standing and sitting modes, a database was generated that contained the possible standing and sitting scenarios as outlined in Table 4-3. The data acquired was used for designing the GMM classifiers and finding the optimal voting length for real-time controller switching. For the standing mode, two activities were considered: static and dynamic standing. The former consists of activities in which the subject stands still such as standing stationary and shifting weight between the limbs. The latter contains

more active movements, such as taking small steps, turning in place, and repositioning the limb. For each of the static and dynamic standing activities, four 100-second trials were measured of which the middle 80 seconds were used for generation of the database. From the first two trials, 200 frames with random initial points for four different frame lengths, *f*, of 50, 100, 200, and 400 samples were extracted to generate the features for the GMM classifier. The remaining standing trials were used for voting vector length determination.

Table 4-3. Different activity scenarios for database generation.

Scenario	#. of trials	Activity Mode	Activity	Purpose
1	4	Standing	Static Standing	GMM, OVVL
2	4	Standing	Dynamic Standing	GMM, OVVL
3	15	Sitting	Standing Up	GMM
4	15	Sitting	Sitting Down	GMM
5	2	Sitting	Sitting	OVVL

Note. GMM stands for the task of designing the GMM classifier. OVVL stands for the task of finding the optimal voting vector length for real-time controller switching.

Generation of the database for the sitting mode was more complicated, since the finite state based impedance controller for sitting includes the SU and SD transitions. These transitions are initiated by the intent recognizer. Without a database containing these transitions, the intent recognizer cannot be designed. In order to overcome this problem, the SU and SD transitions were triggered using knee angle thresholds for generating the database. For generating the database, an activity mode change occurs during standing up in sitting mode to standing mode when the knee angle becomes less than 5 degrees. For sitting down, the finite state based impedance controller is switched to sitting mode when the knee angle

exceeds 5 degrees. Fifteen trials for both cases are conducted. The four seconds after the sitting down transition and four seconds before the SU transition are recorded for generating the feature frames for the GMM classifier design. From each trial 20 frames of length 50, 100, 200 and 400 samples are generated. Moreover, two 100-second sitting trials were recorded for finding the optimal voting vector length for sitting to standing transitions. During these trials, the subject sat on a stool, did sitting activities such as repositioning limbs, changing orientation, and reaching an object excluding SU transition. For each frame length, the database for the GMM classifier design included 800 frames of standing data and 600 frames of sitting data.

Feature Extraction

The real-time nature of the problem requires that the features extracted from the seven prosthesis signals be computationally inexpensive, and as such, the mean and standard deviation were selected as features to extract from each frame, resulting in 14 fundamental simple time domain features. After the features were extracted, they were normalized into the range of [-1, 1] to eliminate the scaling effects between different features. Balancing the information content of a frame against frame length is important since additional delay for intent recognition is introduced as the frame size grows. In order to find the optimal frame length, different frame sizes (50, 100, 200 and 400 samples) were considered.

Dimension Reduction

In order to decrease the time required for real-time intent recognition and training and prevent over-fitting, the feature space was reduced (at the cost of information content) using Principal Component Analysis (PCA) [14] and Linear Discriminant Analysis (LDA) [15], from 14 dimensions to a feature space of 1, 2

and 3 dimensions. Both approaches employ linear transformations, which only necessitate a matrix multiplication operation. Since orthonormal transformations tend to decrease the magnitude of the elements in the transformed matrix as compared to the initial matrix, the reduced features are normalized into the range of [-1, 1] to avoid any possible numerical instability in the GMM classification phase.

Gaussian Mixture Model Activity Mode Classification

Gaussian Mixture Models (GMM) are used to characterize the probability that the user and prosthesis is engaged in a given activity mode. Specifically, a separate GMM is used to describe each activity mode, w_i. For some set of inputs $\vec{x}$, the probability of being in an activity mode, w_i, is given by:

$$p(\vec{x} \mid w_i) = \sum_{k=1}^{K} \lambda_k^i \, p_k^i(\vec{x}) \tag{1}$$

where

$$p_k^i(\vec{x}) = \frac{1}{\sqrt{(2\pi)^D \left|\sum_k^i\right|}} \exp\left\{-\frac{1}{2}(\vec{x}-\vec{\mu}_k^i)'(\sum_k^i)^{-1}(\vec{x}-\vec{\mu}_k^i)\right\} \tag{2}$$

where K is the number of components of the mixture model, λ_k^i is the mixture parameter of the i^{th} GMM for the k^{th} component, which satisfy the constraints $\sum_{k=1}^{K} \lambda_k^i = 1$ and $\lambda_k^i \geq 0$. The mixture component, $p_k^i(\vec{x})$, is a multivariate Gaussian probability density function with a $D \times 1$ mean vector, $\vec{\mu}_k^i$, and $D \times D$ full covariance matrix, $\sum_k^i$, with $D(D+1)/2$ free parameters. Each GMM can be parameterized by $K(1+D+D(D+1)/2)-1$ parameters, which are the mixture parameters, mean vectors and covariance matrices, notated as $w_i = \{\lambda_k^i, \vec{\mu}_k^i, \sum_k^i\}$. Once the GMM's are parameterized, for a given sample feature vector, $\vec{x}_S$, the activity mode, w_m, is selected as the mode with the highest probability:

$$w_m = \arg\max_{w_i}(p(\vec{x}_S \mid w_i)) . \tag{3}$$

Parameterization of the GMM's for all desired activity modes is achieved based on training data in an

iterative fashion with the Expectation Maximization (EM) algorithm [16]. Several initialization schemes for EM are suggested in [17]. In this work, the reduced dataset for an activity mode, w_i, is roughly clustered using the k-means algorithm [18]. These clusters are used to initialize the EM algorithm for finding the mixtures. A key factor affecting the classification performance of GMM's is the number of mixture components, K. As such, the performance of the models for a range of mixture components should be considered and compared for a given application.

Model Selection

The model search space consists of 42 models, which in turn consist of 6 dimension methods (i.e., PCA and LDA for 1 to 3 dimensions) applied to 7 GMM models ranging from order 2 to 8, for each frame length. In order to find the best classifier for each frame length, the Area under the Receiver Operator Characteristics curve (AUC) [19] is used as the performance metric. The reason for choosing AUC is twofold. Firstly, it provides a comprehensive metric that computes true and false positives for all possible classification thresholds observed in the data. Secondly, the AUC metric is insensitive to class distribution. 10-fold cross-validation (CV) [20] is employed to avoid over-fitting. In 10-fold CV, the data is split into 10 sets of size $N/10$. For purposes of model selection, the classifier is trained on 9 datasets and tested for the AUC on the remaining one. This is repeated ten times until all the data splits are tested and the mean AUC score is recorded as the performance metric of a specific classifier.

Voting Scheme for Controller Mode Switching

The activity mode intent recognizer is a component of the supervisory controller for the powered prosthesis and has two performance objectives. The first objective is to switch to another mode in the

shortest time possible when a mode transition occurs, and the second objective is to avoid switching to another mode when there is no real transition. With respect to the first objective, a longer switching time will decrease the quality of movements since the user will have a perceived latency of the assistance from the prosthesis. However, failure to meet the second objective could have more severe consequences (i.e. causing loss of balance and even a fall). Therefore, to increase assurance of correct mode switching, a voting scheme is used.

In the real-time implementation, overlapping frames are classified at each 10 ms interval (Δt). In the voting scheme, the last *l* classifier decisions are stored in a voting vector and mode switching occurs if more than 90 percent of the classification results are in agreement. To avoid chattering during transition and increase the robustness of the powered prosthesis control, a rule was introduced to not allow the controller mode to switch for 500 ms after a mode switching occurs.

The combination of the voting length, *l,* and the frame length, *f,* determines the delay of activity mode intent recognition. To optimize the voting vector length, *l,* the last two trials for each scenario in the experimental database were used. In this process, the real-time activity intent recognizer is implemented offline with possible voting vector length from 10 to 100 in increments of 10. For a specific frame length, *f*, the smallest voting length, l_s, which does not switch to standing for the sitting trials and to standing for sitting trials, is selected as the optimal voting vector length.

Once the optimal voting length for each frame is found, the best frame length for the real-time activity intent mode recognition needs to be determined. It is assumed that the two trials for each scenario encompass all the possible cases and the best models for each frame length are reliable, meaning they do not result in incorrect controller switching. Hence, the problem becomes to select the frame length which

yields the least amount of delay, *d,* in the intent recognition. This is accomplished by computing an approximate delay score, $d = f/2 + 10l$, for each frame length.

Results and Discussions

Real-time Intent Recognition

The intent recognition analysis returns the GMM with 6 mixtures using three dimensional PCA reduction using 100 sample frames as the best model. The voting vector length for this model is 40 resulting in an approximate delay of 450 ms. Surface plots of the standing and sitting GMMs showing the regions of the feature space with greater than 0.05 probability densities are presented in Fig. 4-5. The distinct locations of the two different activities in the reduced feature space can be seen in this figure. It should be noted that the SU and SD transitions look like a bridge connecting the standing and sitting modes in this plot. The best model (the model with the least delay) is used for real-time intent recognition between the standing and sitting activity modes. Five trials lasting 90 seconds were conducted to verify that the supervisory controller works in a closed feedback loop. During each trial, the experimenter gave audio cues to the subject to stand up and sit down. During the five trials, no erroneous mode changes were observed. The prosthetic knee angle and the activity mode for one of the trials are shown in Fig. 4-6. The subject stated that there was no perceived latency during transitions. This also agrees with the fact that the knee trajectories for SU and SD transitions are smooth. One might argue that instead of designing a complex intent recognizer a simple thresholding scheme such as implemented for the database generation might suffice for initiating SU and SD transitions. As can be observed from Fig. 4-6, however, the knee angle threshold used for generating the database (5 degrees) is exceeded many times during standing. If this threshold were used, many

incorrect stand-to-sit transitions would be initiated. The intent recognizer creates an intricate switching function combining many measurements which results in a robust supervisory controller.

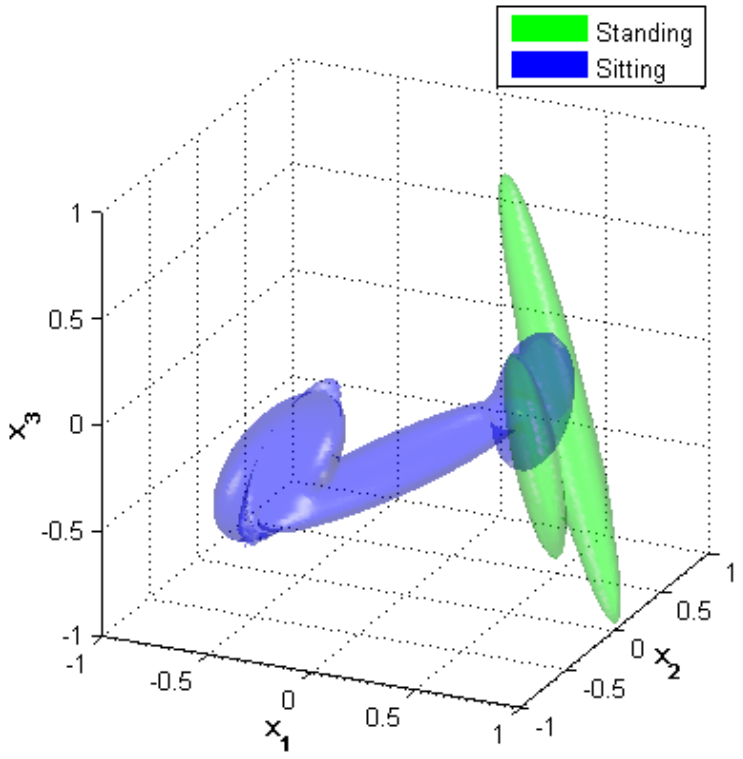

Figure 4-5. Gaussian Mixture Model surface plots of the standing and sitting modes showing the regions of the feature space, where the probability density function is greater than 0.05, for the three dimensional PCA reduced data.

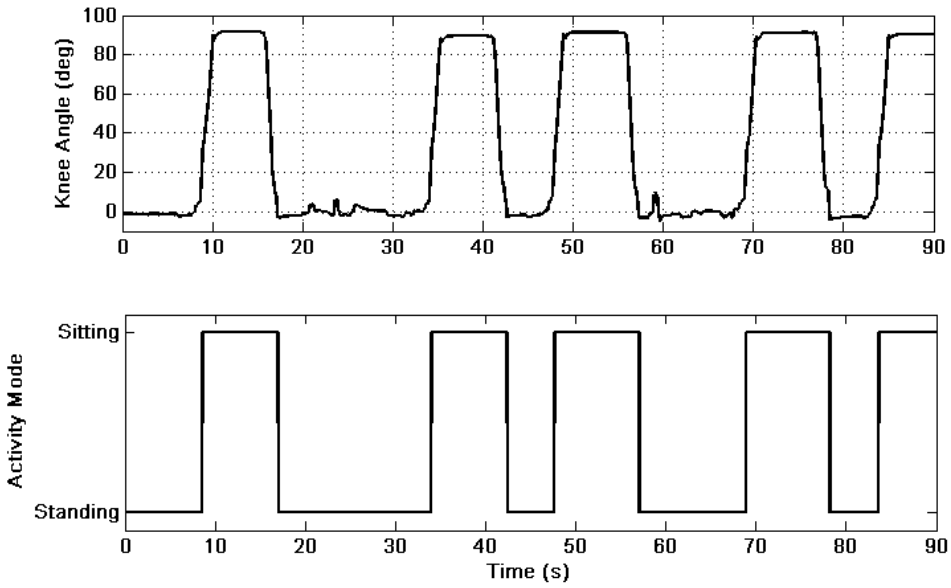

Figure 4-6. Prosthetic knee angle (top) and the real-time activity mode switching (bottom) for a 90 seconds standing and sitting trial.

Biomechanical Evaluation

The knee and ankle angles, torques and powers are shown in Figs. 4-7 and 4-8 for SU and SD, respectively. The corresponding video frame plot showing the middle two second period of these transitions are in Fig. 4-9. In standing up, the prosthesis generates peak torque of around 25 Nm and positive peak power of 50 W at the knee during SU. During SD, a smooth descent with up to 50 W of power dissipated at the knee is observed. Even though no significant power and torque was registered at the ankle, the active ankle joint increases stability by adjusting the ankle angle to keep the foot flat during the SU and SD transitions. It should be noted that the powered prosthesis is capable of generating higher torques than those in Figs. 4-7 and 4-8 but the parameters were tuned such that the subject feels most comfortable. The relatively short residual limb length of the subject could limit the maximum comfortable knee torque during SU. The subject stated while using the powered prosthesis it was easier for him to stand up and he feels

more support from the prosthesis relative to using his passive one. Presumably, the increased support from the powered prosthesis reduced the joint torques and powers required during standing up from the sound side, although these were not measured in the experimental trials.

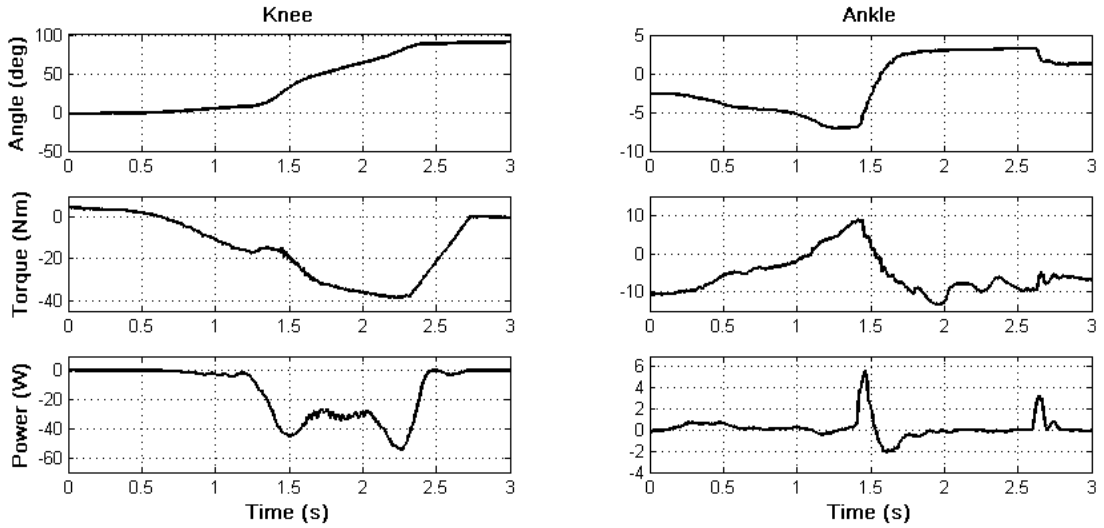

Figure 4-7. Knee and ankle angles (top), torques (middle) and powers (bottom) during sitting down.

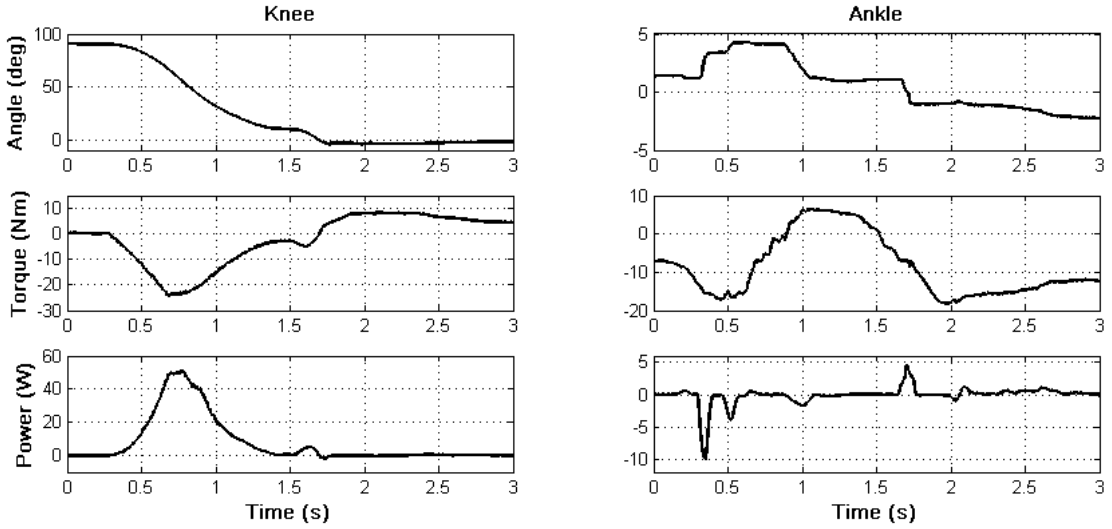

Figure 4-8. Knee and ankle angles (top), torques (middle) and powers (bottom) during standing up.

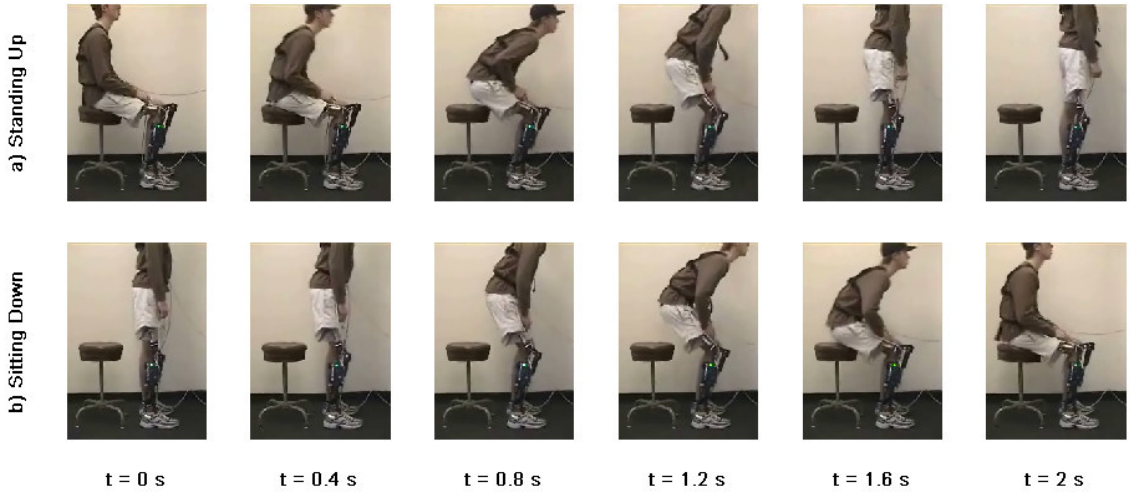

Figure 4-9. Video frames of standing up (a) and sitting down (b) transitions.

Conclusion

This paper describes a novel control framework for standing and sitting down with a powered knee and ankle prosthesis. The results indicate that the high level controller (intent recognizer) infers user's intent without perceived latency by the user and switches the underlying controllers correctly. Operating in the proposed control framework, the powered prosthesis was able contribute significant net power to the user at the knee joint during standing up that could not have been achieved with passive prostheses. Further work includes comprehensive biomechanical evaluation of the assistive sit-to-stand and stand-to-sit control framework on multiple amputee subjects.

References

[1] U. Lindemann, H. Claus, M. Stuber, P. Augat, R. Muche, T. Nikolaus, and C. Becker, "Measuring power during the sit-to-stand transfer," *European J. of Applied Physiology,* vol. 89, no. 5, pp. 466-470, Jun, 2003.

[2] M. Galli, V. Cimolin, M. Crivellini, and I. Campanini, “Quantitative analysis of sit to stand movement: Experimental set-up definition and application to healthy and hemiplegic adults,” *Gait & Posture,* vol. 28, no. 1, pp. 80-85, Jul, 2008.

[3] A. Kralj, R. J. Jaeger, and M. Munih, “Analysis of Standing up and Sitting down in Humans - Definitions and Normative Data Presentation,” *J. of Biomechanics,* vol. 23, no. 11, pp. 1123-1138, 1990.

[4] W. G. M. Janssen, H. B. J. Bussmann, and H. J. Stam, “Determinants of the sit-to-stand movement: A review,” *Physical Therapy,* vol. 82, no. 9, pp. 866-879, Sep, 2002.

[5] M. Schenkman, R. A. Berger, P. O. Riley, R. W. Mann, and W. A. Hodge, “Whole-body movements during rising to standing from sitting,” *Physical Therapy,* vol. 70, no. 10, pp. 638-648, Oct, 1990.

[6] H. Burger, J. Kuzelicki, and C. Marincek, “Transition from sitting to standing after trans-femoral amputation,” *Prosthetics and Orthotics International,* vol. 29, no. 2, pp. 139-151, Aug, 2005.

[7] D. Berry, “Microprocessor prosthetic knees,” *Phys Med Rehabil Clin N Am,* vol. 17, no. 1, pp. 91-113, vii, Feb, 2006.

[8] W. C. Flowers, and R. W. Mann, “Electrohydraulic knee-torque controller for a prosthesis simulator,” *ASME J. of Biomechanical Engineering,* vol. 99, no. 4, pp. 3-8, 1977.

[9] D. Popovic, and L. Schwirtlich, “Belgrade active A/K prosthesis,” in de Vries, J. (Ed.), Electrophysiological Kinesiology, Intern. Congress Ser. No. 804, Excerpta Medica, Amsterdam, The Netherlands, pp. 337-343, 1988.

[10] S. Bedard, and P. Roy, *Actuated Leg Prosthesis for Above-Knee Amputees*, U. S. Patent, 2003.

[11] E. Martinez- Villalpando, J. Weber, G. Elliott, and H. Herr, “Design of an agonist-antagonist active knee prosthesis,” *Proc. IEEE/RAS-EMBS Int. Conf. on Biomedical Robotics and Biomechatronics*, pp.

529-534, 2008.

[12] F. Sup, H. A. Varol, J. Mitchell, T. Withrow, and M. Goldfarb, “Design and control of an active electrical knee and ankle prosthesis,” *Proc. IEEE/RAS-EMBS Int. Conf. on Biomedical Robotics and Biomechatronics*, pp. 523-528, 2008.

[13] H. A. Varol, F. Sup, and M. Goldfarb, “Real-time gait mode intent recognition of a powered knee and ankle prosthesis for standing and walking,” *Proc. IEEE/RAS-EMBS Int. Conf. on Biomedical Robotics and Biomechatronics*, pp. 66-72, 2008.

[14] I. T. Jolliffe, *Principal Component Analysis*, 2nd ed., New York: Springer, 2002.

[15] R. A. Fisher, “The statistical utilization of multiple measurements,” *Annals of Eugenics,* vol. 8, pp. 376-386, 1938.

[16] A. P. Dempster, N. M. Laird, and D. B. Rubin, “Maximum likelihood from incomplete data via EM algorithm,” *J. of the Royal Statistical Society Series B-Methodological,* vol. 39, no. 1, pp. 1-38, 1977.

[17] G. J. McLachlan, and D. Peel, *Finite mixture models*, New York: Wiley, 2000.

[18] J. A. Hartigan, and M. A. Wong, “A K-means clustering algorithm,” *Applied Statistics,* vol. 28, no. 1, pp. 100-108, 1979.

[19] T. Fawcett, “An Introduction to ROC Analysis,” *Pattern Recognition Letters,* vol. 27, no. 8, pp. 861-874, Jun, 2006.

[20] T. M. Mitchell, *Machine Learning*, New York: McGraw-Hill, 1997.

CHAPTER V

Slope Ascent with a Powered Knee and Ankle Prosthesis

Note: The work presented in this chapter will be combined with the supervisory controller for cadence and slope estimators and submitted to IEEE Transactions on Neural Systems and Rehabilitation Engineering.

Abstract

This paper extends the functionality of a powered knee and ankle prosthesis previously developed by the authors by incorporating a slope ascent controller to the control architecture. The powered prosthesis employs a finite-state impedance control framework to coordinate user prosthesis interaction. Results with a unilateral transfemoral amputee demonstrate that near normal gait on slopes of 5 and 10 degrees can be achieved with the proposed control and powered prosthesis. Increases in knee flexion and ankle dorsiflexion during stance are observed relative to level walking. Power consumption measurements indicate the device consumes 45, 60 and 72 W for level, 5, and 10 degrees upslope walking.

Introduction

In daily living, walking on inclined surfaces is a frequently encountered activity which requires significant coordination and power in the lower limbs. With respect to kinematics, upslope walking necessitates an increased range of motion at the hip, knee and ankle joints as compared to level ground walking [1]. The maximum moments and powers observed at the knee and hip joints correlate closely with increasing slope angle [2]. This trend is also observed at the ankle to a lesser extent [2]. Furthermore, there is an upward trend in metabolic cost of transport corresponding with steeper grades of inclines [3].

Presently, most commercial lower limb prostheses are passive devices and are unable to deliver net power. This loss of net power generation at the lower limb impairs the ability of the prosthesis to restore biomechanically normal level, walking up stairs and slopes, and rising from the seated position [4-10]. In the absence of net power generation at the knee and ankle, transfemoral amputees with passive prostheses have been shown to expend 60% more metabolic energy [10] and exert three times the affected-side hip power and torque [5] when compared to healthy subjects during level walking. When walking on inclines, transfemoral amputees cannot achieve knee flexion in the prosthetic knee and must compensate by altering their gait patterns [4]. Since inclined walking is more demanding in regards to the kinetics and energy expenditure compared to level walking [3], the difficulties faced by amputee in upslope walking will be exacerbated. Presumably, introduction of power to lower limb prostheses might alleviate the difficulties confronted by amputees while walking up slopes.

Active prosthesis development aimed to return mobility and functionality to amputees dates back to the early 1970's with a tethered electro-hydraulically actuated knee joint. This prosthesis served as a test bed for studying the feasibility of powered knee joints during walking [11]. More recently, Ossur, a prosthetics company, introduced a powered knee prosthesis that is capable of generating net active power. The device provides stance assistance for stair and slope ascent and a powered swing [12]. Work in powered transtibial prostheses includes the "Proprio Foot" developed by Ossur, the "powered" ankle prosthesis does not contribute net power to gait, but rather adjusts the ankle angle to accommodate ground slope during swing. While sitting, the device adjusts the ankle angle to better accommodate sitting posture [13]. Bellman et al. describe an active robotic ankle prosthesis with actuated degrees of freedom in both the sagittal and frontal planes [14]. Au and Herr built a powered ankle-foot prosthesis that incorporates both parallel and

series elasticity to reduce peak motor torque and power requirements and to provide a more suitable output impedance [15]. The authors were not able to find any scientific literature on slope ascent for any of these active lower limb prostheses.

The authors have previously developed a powered knee and ankle prosthesis with the primary goal of restoring normal locomotive functions to transfemoral amputees [16]. This work demonstrated the potential of such a device to restore near normal gait patterns and increase self-selected walking speed of a transfemoral amputee on level ground relative to a daily-use passive prosthesis. The device has been successfully demonstrated in walking, standing, sitting and sit-to-stand and stand-to-sit transitions [16-18]. Within the previously developed control framework, the present work demonstrates the extension of the walking controller to inclined slopes. The paper is organized as follows. Firstly, the control framework for the powered prosthesis is detailed. Secondly, the extension of the control to accommodate slope ascent is explained. Thirdly, an overview of the powered prosthesis used in this study and the experimental protocol is presented. Lastly, biomechanical results with a transfemoral amputee walking upslope over ground are reported and discussed.

Methodology

Control Architecture

The powered prosthesis operates with a three level control hierarchy, as diagrammed in Fig. 5-1. The high level supervisory controller, which is the intent recognizer, infers the user's intent based on the interaction between the user and the prosthesis, and correspondingly switches the middle level controllers, as described in [17, 18]. Additionally, the high level controller estimates ground slope with an accelerometer

mounted on the foot of the prosthesis and cadence by observing the timing of the ground reaction forces. A middle level controller is developed for each activity mode, such as walking, standing, sitting, and stairs. The middle level controllers generate torque references for the joints using a finite state machine that modulates the impedance of the joints depending on the phase of the activity. The low-level controllers are the closed-loop joint torque controllers, which compensate for the transmission dynamics (i.e., primarily friction and inertia), and thus enable tracking of the knee and ankle joint torque references (commanded by the middle level controllers) with a higher bandwidth and accuracy than is afforded with an open-loop torque control approach. In this work, the walking mode finite state impedance based controller is extended to accommodate ascending two levels of inclination.

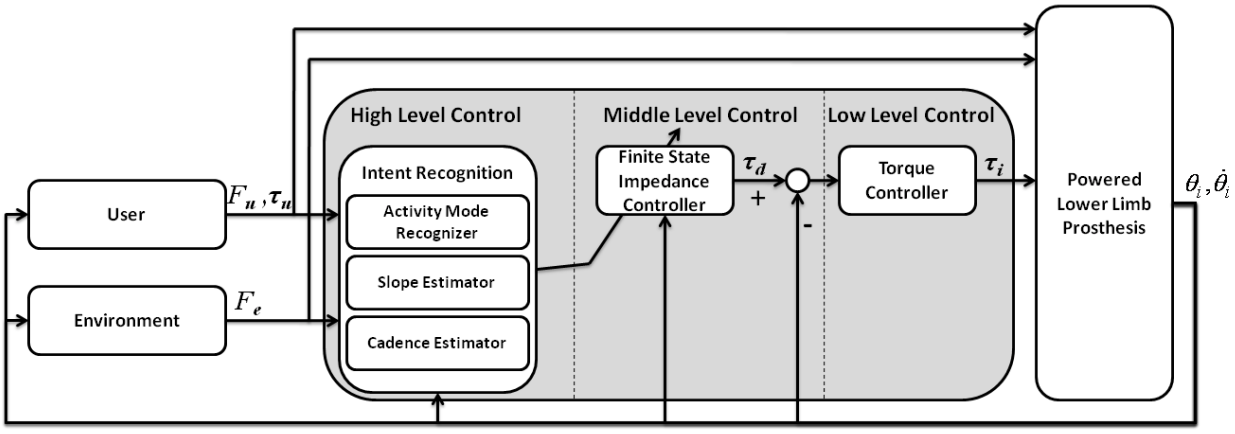

Figure 5-1. Powered prosthesis control architecture.

Finite State Based Impedance Control

In the finite state impedance based control, the impedance behavior of healthy biomechanical gait is mimicked by modulating joint impedances of the prosthesis according to the phase of gait. The knee and ankle torques, τ_i, are described in each phase by a passive spring and damper with a fixed equilibrium point,

given by:

$$\tau_i = k_i(\theta - \theta_{ki}) + b_i\dot{\theta} \quad (1)$$

where k_i, b_i, and θ_{ki} denote the linear stiffness, damping coefficient, and equilibrium point, respectively, for the i^{th} state. Switching joint impedances between the gait phases is initiated by biomechanical cues, such as heel strike or the changing from knee flexion to extension during swing. The approach requires the development of a state machine for each type of user activity such as walking, standing, sitting, and stair ascent and descent. In particular, the state model for walking, Fig. 5-2, is described by five phases, three of which are stance phases (early stance, middle stance, and late stance) and two of which are swing phases (swing knee flexion and swing knee extension). The result is an effective and predictable controller that does not violate passive behavior except when the user requests active power transfer by triggering a transition. The authors previously developed controllers for standing, level walking for different speeds, and sitting [16-18].

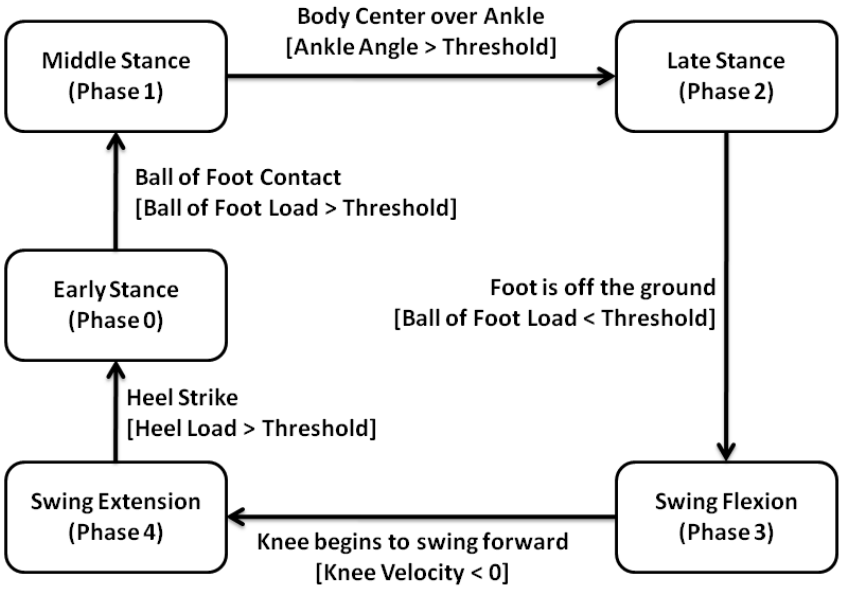

Figure 5-2. The state chart depicting the phase transitions in walking mode.

Phase 0 begins at heel strike, upon which the knee immediately begins to flex to provide impact absorption and initiate the loading response. Simultaneously, the ankle plantarflexes to reach a flat foot state. Both knee and ankle joints have moderate stiffness during this mode to prevent buckling and allow for knee stance flexion. The length of Phase 0 is directly related to the threshold value for ball of the foot contact. Phase 1 increases the stiffness of the knee and ankle joints to provide support and allow for loading of the ankle joint. Phase 2, the push-off phase, begins as the ankle dorsiflexes beyond a given angle (i.e. user's center of mass lies forward of stance foot). The knee stiffness decreases in this mode to allow knee flexion while the ankle provides a plantarflexive torque for push-off. Phase 3 begins as the foot leaves the ground and lasts until the knee reaches maximum flexion. Phase 4 is active during the extension of the knee joint (i.e. as the lower leg extends), which begins as the knee velocity becomes negative and ends at heel strike. In both of the swing phases, the ankle torque is small and is represented in the controller as a (relatively) weak spring regulated to a predefined angle to allow for toe clearance. The knee is modeled

as a damper with a weak spring regulated to flexed position in both swing phases.

Upslope Walking

The biomechanics at the knee and ankle joints of walking at a self-selected speed up a slope do not change significantly as compared with level walking [1], Fig. 5-3. Comparing upslope biomechanics to level walking, it is observed that the knee flexion is increased at heel strike to compensate for the elevation change. Stance flexion behavior is similar to level walking, but only having offset due to the increased knee flexion at heel strike. At middle stance, the knee extends more than level walking in order to lift the body. In late swing, knee extension ends at a higher angle to compensate for the elevation change anticipated at heel strike. The knee joint moment exhibits an increase in both the early stance extensor torque and the middle stance flexor torque. It might be hypothesized that increased knee torques are instrumental in the raising the body up the incline. At the ankle joint, dorsiflexion is increased during stance to conform to the ground slope and in late stance plantarflexion is increased to maintain ground contact. The ankle torques for level walking and upslope walking do not show any major differences. The trends presented in Fig. 5-3 are maintained for slopes of less than 9 deg, but the scaling is not linear with respect to the slope. Due to the similarity of the gait patterns for level and upslope walking, the previously developed walking impedance controller structure is used to accomplish upslope walking.

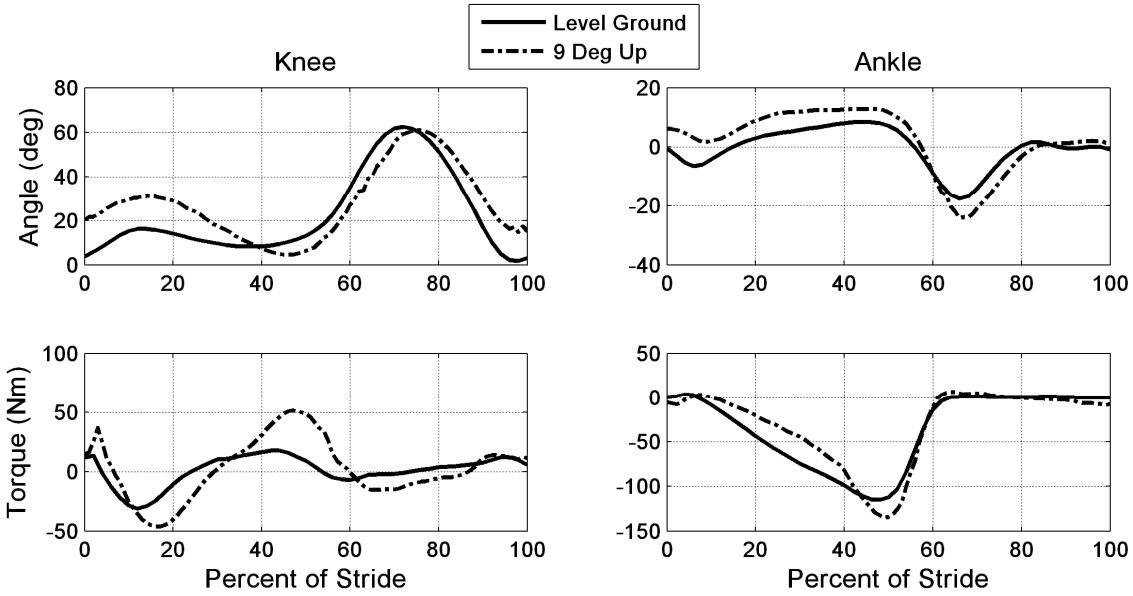

Figure 5-3. Comparison of normal biomechanical gait data for level [5] and upslope walking, 9 deg, [1] joint angles and torques at the knee and ankle for a 75 kg subject.

Experimental Setup

Powered Prosthesis

Previously, the authors have described a self-contained powered knee and ankle prosthesis [16], Fig. 5-4, that was used for the upslope walking testing, described herein. The 4.2 kg prosthesis is a two degree of freedom robotic device capable of generating human-scale torque and power at the knee and ankle joints. Actuation of each joint is accomplished via slider-crank linkages driven by motor ball screw assemblies. The ankle actuation unit incorporates a spring to bias the motor's axial force output toward ankle plantarflexion, and to supplement power output during ankle push off. The device's sensor package includes a custom load cell to measure the sagittal socket interface moment above the knee joint, a custom foot to measure the ground reaction force at the heel and ball of the foot, and commercial potentiometers and load cells to measure joint positions and torques, respectively. The self-contained version hosts an

embedded system allowing for both tethered and untethered operation run by either MATLAB Simulink or a PIC32 microcontroller, respectively. The prosthesis is powered by a 118 W·h lithium polymer battery.

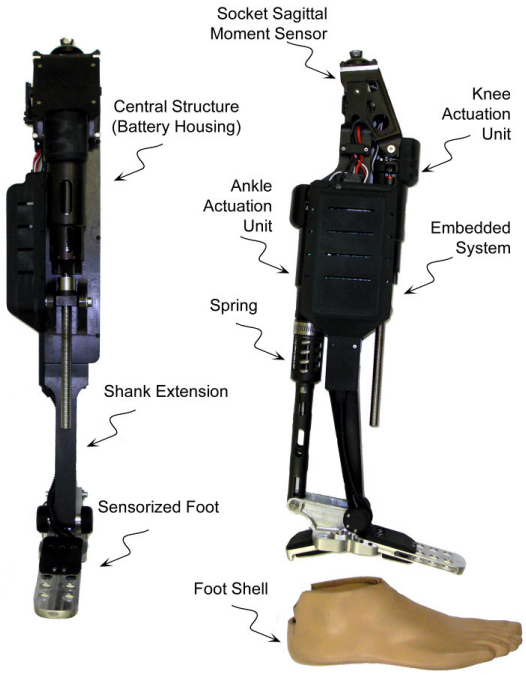

Figure 5-4. The self-contained powered knee and ankle transfemoral prosthesis.

Experimental Subject

The prosthesis was tested on a 20-year-old male (1.93 m, 70 kg) unilateral amputee four years post amputation, Fig. 5-5. The length of the test subject's residual limb, measured from the greater trochanter to the amputated site, was 55% of the length of the non-impaired side measured from the greater trochanter to the lateral epicondyle. The subject uses an Otto Bock C-leg with a Freedom Renegade prosthetic foot for daily use. The subject's daily use socket was used in all experiments, where the powered prosthesis prototype was attached in place of the daily use prosthesis. The overall prosthesis height and varus-valgus alignment were performed by a licensed prosthetist. The prosthesis has been previously tuned for level

walking at different speeds, standing and sitting modes for the subject. The subject spent over 200 hours of time using the prosthesis in a laboratory setting and was proficient in using the device in the previously mentioned activities.

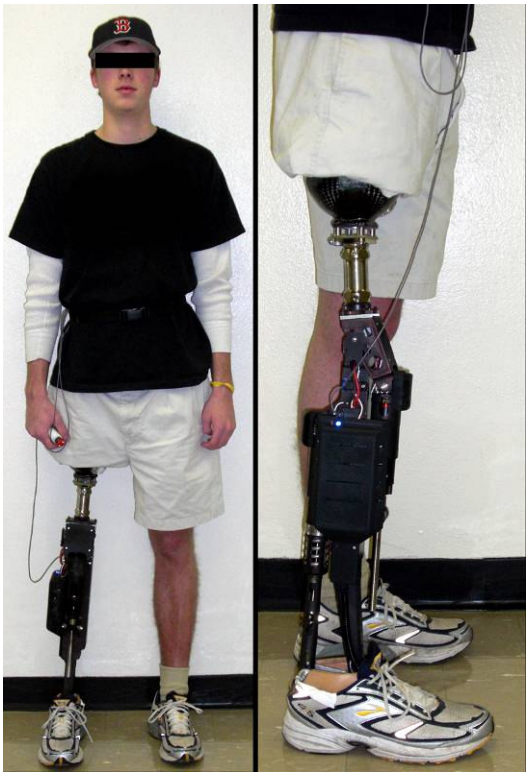

Figure 5-5. Unilateral transfemoral amputee test subject used for the powered prosthesis evaluation.

Experimental Procedure

For this paper, the inclinations of 5 and 10 degrees were selected. According to [19], the building codes in the United States state the maximum incline of a ramp cannot exceed a slope of 1:12 which corresponds to 5 degrees. The gait biomechanics of ascending slopes of less than 10 deg do not require excessive hip torques [1] that may exceed the capabilities of an amputee's affected side. The impedance parameters of the powered prosthesis are tuned using a combination of feedback from the user and visual inspection of

the joint angle, torque, and power data. First, the prosthesis was tuned for self-selected speed level ground walking. In this tuning process, two objectives were considered. The first objective was to achieve healthy biomechanical gait patterns as shown in level walking data presented in [5]. The second objective was to decrease the effort based on the qualitative feedback from the subject. Starting with the level ground parameters, the prosthesis was tuned for the subject for 5 deg upslope walking in an iterative manner. For upslope walking, the biomechanical gait patterns were compared with upslope walking as presented in [1]. Once the tuning process was finished for the five degree upslope walking, those parameters were set as the initial 10 deg parameters and the above process was repeated. The experimentally tuned parameters for each ground slope are presented in Table 5-1. For these experiments, knee and ankle joint angles, torques and powers for the prosthesis were collected. In addition, electrical power consumption of the device at the knee and ankle were measured via onboard sensors.

Table 5-1. Impedance parameters for walking from experimental tuning.

		Knee Impedance			Ankle Impedance		
Phase	Slope Deg	K Nm deg^{-1}	b N s m^{-1}	θ_k deg	k Nm deg^{-1}	b N s m^{-1}	θ_k deg
0	0	2.5	0.05	10	4.0	0.04	1
	5	1.5	0.07	18	4.0	0.06	2
	10	0.8	0.1	35	4.0	0.09	3
1	0	5.0	0.06	10	5.0	0.04	0
	5	4.0	0.06	13	5.0	0.04	0
	10	3.5	0.1	19	5.0	0.04	3
2	0	5.0	0.02	14	5.0	0.01	-16
	5	4.0	0.06	16	5.0	0.01	-18
	10	4.0	0.05	19	5.0	0.01	-22
3	0	0.1	0.03	65	0.6	0.05	2
	5	0.1	0.03	65	1.0	0.05	6
	10	0.2	0.03	60	2.0	0.03	12
4	0	0.3	0.01	45	1.0	0.03	3
	5	0.4	0.02	45	1.5	0.03	9
	10	0.6	0.02	50	2.5	0.03	15

Results and Discussion

The subject walked on the powered prosthesis for 20 m on level, 5 and 10 degree inclines at a self-selected cadence (90, 93, and 95 steps/min, respectively). Averaged joint angles, torques and powers from walking on each inclination for ten consecutive strides are shown in Fig. 5-6. At the knee joint, flexion increases at early and middle stance as well as in late swing to accommodate an increased ground slope. The increased knee flexion in the prosthesis mimics the normal biomechanics of inclined walking and potentially alleviate the problems faced by amputees in upslope walking [4]. Compared to level walking, the knee joint torques exhibit a decreased extensive torque at middle stance and an increased flexive torque of up 50 Nm in late stance, corresponding to the ground slope. At 5 and 10 degrees, the knee generated power up to 50 W and shows an increase over level ground in middle and late stance. Increasing ground

slope also translates into increased ankle joint dorsiflexion in early and middle stance and increased plantarflexion in late stance. During swing, the ankle joint assumes a more dorsiflexed position corresponding to increasing ground slope. The ankle torque is more plantarflexive during middle stance with torques over 100 Nm achieved. Power at the ankle joint approaches 200 W during late stance. For each stride, the prosthesis delivers 13.7, 16.1 and 18.5 J of net energy on average at the ankle for level, 5 and 10 degrees, respectively. It should be noted that even though no joint trajectories have been dictated by the finite state impedance controller, the joint angles created as a result of the user prosthesis interaction show consistency, but allow for stride by stride variance, Fig. 5-7. During the level and ascent trials, the subject stated he felt a decreased level of exertion while using the powered prosthesis as compared with his daily use prosthesis. He stated that the primary differences between his daily use and powered prosthesis were active ankle push-off, powered knee swing phase and maintaining foot flat on sloped surfaces.

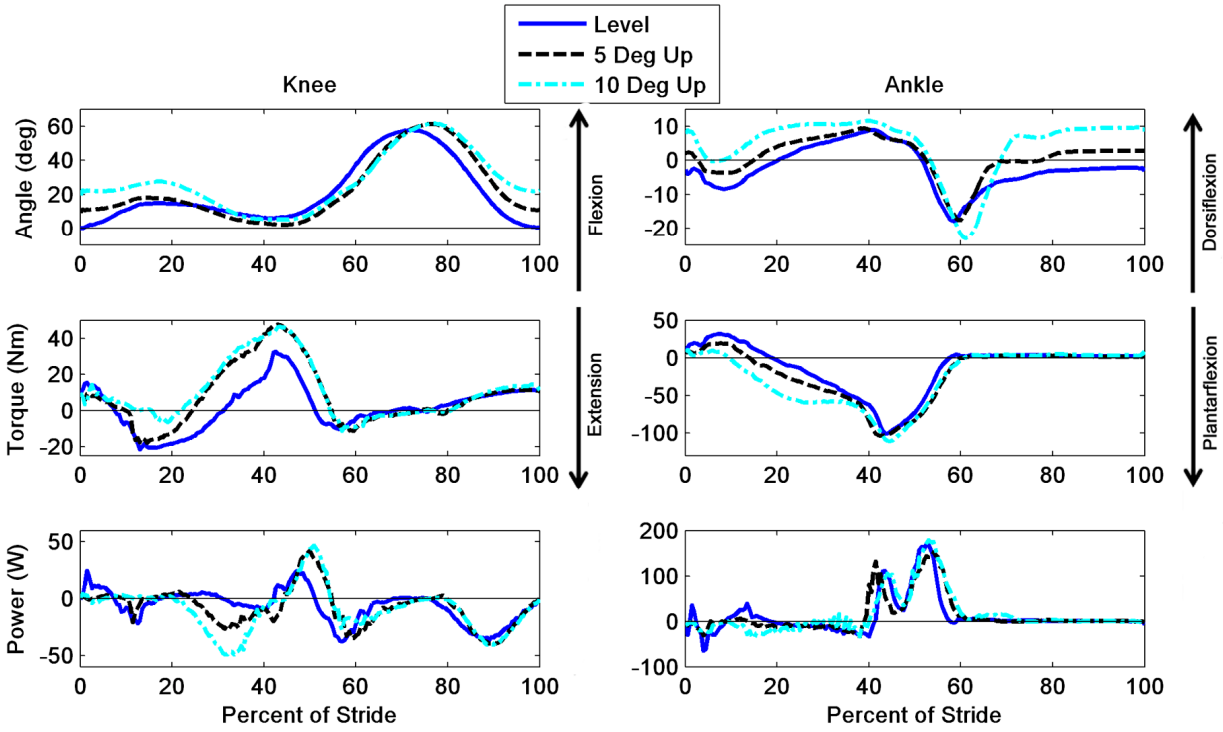

Figure 5-6. Averaged joint angles, torques and powers of the powered prosthesis for ten consecutive gait cycles at self-selected speed for level, 5, and 10 degrees walking.

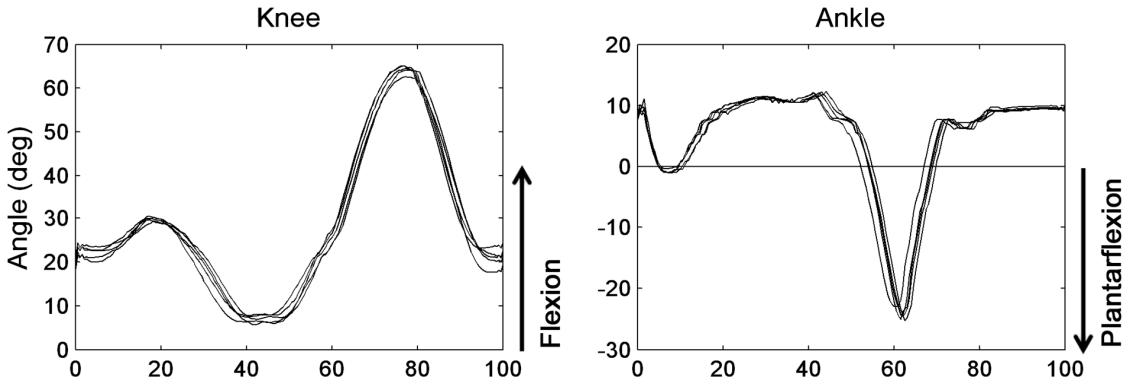

Figure 5-7. Measured joint angles of the powered prosthesis for five consecutive gait cycles at self-selected speed for 10 degrees upslope walking.

Power consumption is one of the primary bottlenecks in advancing current powered prosthesis technology. In order to test the feasibility of this work beyond a laboratory setting, the electrical power

requirements are investigated. The average electrical power required by the prosthesis (i.e., the embedded system, knee joint, and ankle joint) during level, 5 and 10 degree upslope walking at a self-selected cadence is shown in Fig. 5-8. The total average power consumption for level, 5 and 10 degrees is 45, 60, and 72 W, respectively. Consistent with metabolic energy consumption [3], the powered prosthesis consumes more energy with increasing slope. It should be noted that the device was previously reported to consume 66 W [16] for level walking at self-selected speed. In this work the level walking power consumption is measured to be 45 W. This decrease in power consumption is a combination of improvements in the low level torque control by changing from proportional force control to proportional-derivative controller and improvements in the impedance parameter tuning.

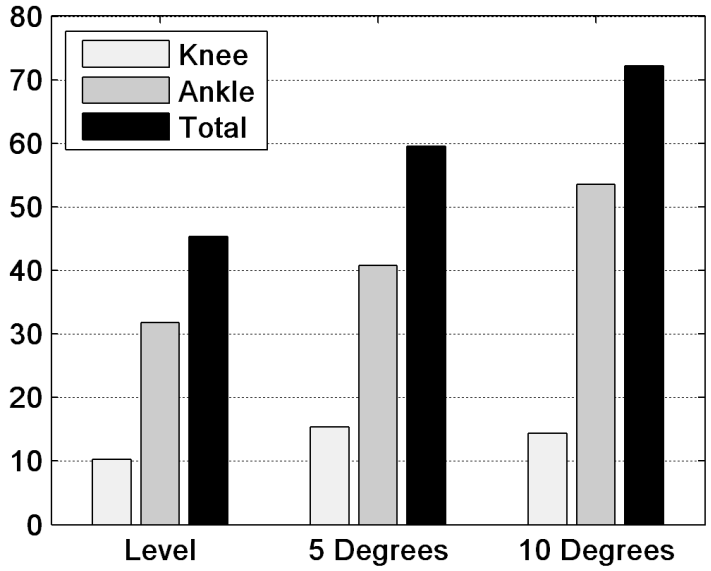

Figure 5-8. Average electrical power consumption of the powered prosthesis for level, 5 deg, and 10 deg upslope walking at self-selected speed on normal ground.

Conclusion

This work presented the extension of the control framework to slope ascent for the powered knee and ankle prosthesis developed in prior works by the authors. The results indicate that the device has the potential to restore near normal gait patterns in unilateral transfemoral amputees. Future work includes comprehensive biomechanical evaluation of the powered prosthesis and the slope ascent controller on multiple amputee subjects.

References

[1] A. N. Lay, C. J. Hass, and R. J. Gregor, “The effects of sloped surfaces on locomotion: a kinematic and kinetic analysis,” J. of Biomechanics, vol. 39, no. 9, pp. 1621-8, 2006.

[2] A. S. McIntosh, K. T. Beatty, L. N. Dwan, and D. R. Vickers, “Gait dynamics on an inclined walkway,” J. of Biomechanics, vol. 39, no. 13, pp. 2491-502, 2006.

[3] A. C. Bobbert, “Energy expenditure in level and grade walking,” J. of Applied Physiology vol. 15, pp. 1015-1021, 1960.

[4] A. H. Vrieling, H. G. van Keeken, T. Schoppen, E. Otten, J. P. K. Halbertsma, A. L. Hof, and K. Postema, “Uphill and downhill walking in unilateral lower limb amputees,” Gait & Posture, vol. 28, no. 2, pp. 235-242, Aug, 2008.

[5] D. Winter, The Biomechanics and Motor Control of Human Gait: Normal, Elderly and Pathological, 2nd ed.: University of Waterloo Press, 1991.

[6] D. A. Winter, and S. E. Sienko, “Biomechanics of below-knee amputee gait,” J. of Biomechanics, vol. 21, no. 5, pp. 361-367, 1988.

[7] H. Burger, J. Kuzelicki, and C. Marincek, “Transition from sitting to standing after trans-femoral amputation,” Prosthetics and Orthotics International, vol. 29, no. 2, pp. 139-151, Aug, 2005.

[8] T. Schmalz, S. Blumentritt, and B. Marx, “Biomechanical analysis of stair ambulation in lower limb amputees,” Gait & Posture, vol. 25, no. 2, pp. 267-278, Feb, 2007.

[9] M. Traballesi, P. Porcacchia, T. Averna, and S. Brunelli, “Energy cost of walking measurements in

subjects with lower limb amputations: A comparison study between floor and treadmill test," Gait & Posture, vol. 27, no. 1, pp. 70-75, Jan, 2008.

[10] R. L. Waters, J. Perry, D. Antonelli, and H. Hislop, "Energy cost of walking of amputees - Influence of level of amputation," J. of Bone and Joint Surgery-American Vol., vol. 58, no. 1, pp. 42-46, 1976.

[11] W. C. Flowers, and R. W. Mann, "Electrohydraulic knee-torque controller for a prosthesis simulator," ASME J. of Biomechanical Engineering, vol. 99, no. 4, pp. 3-8, 1977.

[12] S. Bedard, and P. Roy, Actuated Leg Prosthesis for Above-Knee Amputees, U. S. Patent, 2003.

[13] W. Koniuk, Self-adusting prosthetic ankle apparatus, 6,443,993, U. S. Patent, March, 23, 2001.

[14] R. Bellman, A. Holgate, and T. Sugar, "SPARKy 3: Design of an active robotic ankle prosthesis with two actuated degrees of freedom using regenerative kinetics," Proc. IEEE/RAS-EMBS Int. Conf. on Biomedical Robotics and Biomechatronics, pp. 511-516, 2008.

[15] S. Au, and H. Herr, "Powered ankle-foot prosthesis," IEEE Robotics & Automation Magazine, vol. 15, pp. 52-59, 2008.

[16] F. Sup, H. A. Varol, J. Mitchell, T. J. Withrow, and M. Goldfarb, "Self-Contained Powered Knee and Ankle Prosthesis: Initial Evaluation on a Transfemoral Amputee," IEEE 11th Int. Conf. on Rehabilitation Robotics, pp. 638-644, 2009.

[17] H. A. Varol, F. Sup, and M. Goldfarb, "Real-time gait mode intent recognition of a powered knee and ankle prosthesis for standing and walking," Proc. IEEE/RAS-EMBS Int. Conf. on Biomedical Robotics and Biomechatronics, pp. 66-72, 2008.

[18] H. A. Varol, F. Sup, and M. Goldfarb, "Powered Sit-to-Stand and Assistive Stand-to-Sit Framework for a Powered Transfemoral Prosthesis," IEEE 11th Int. Conf. on Rehabilitation Robotics, pp. 645-651, 2009.

[19] 42 U.S.C. § 12101 et seq., Americans with Disabilities Act of 1990, 1994.

CHAPTER VI

Contributions and Future Work

Contributions

This work aims to develop the technologies required to bring powered knee and ankle prostheses to the commercial market, which in turn, can then bring the benefits of powered prostheses to the amputee population. Specifically, this work accomplishes the following goals.

- Defines the electrical and mechanical power specifications for an active knee and ankle prosthesis.
- Presents a mechanical design for a self-contained, light-weight, electrically powered knee and ankle prosthesis with onboard power, sensing elements and DC motor actuated joints.
- Develops embedded system architecture that enables both tethered and untethered operation of the lower limb prosthesis with onboard computation, signal processing, power management, data logging, and wireless communication.
- Presents the design of compact strain-based sensors to measure the sagittal plane moment above the knee joint and the ground reaction forces at the heel and ball of the foot.
- Describes a general three level control architecture for powered lower limb prostheses. The high level supervisory controller, which is the intent recognizer, infers the user's intent based on the interaction between the user and the prosthesis, and correspondingly switches the middle level controllers. The middle level controllers generate torque references for the joints using a finite state machine that

modulates the impedance of the joints depending on the phase of the activity. The low-level controllers are the closed-loop joint torque controllers.

- Describes the expansion and refinement of the finite-state impedance control structure to accommodate gait at three cadences, standing, slope ascent, sitting and the associated sit-to-stand transitions.
- Presents the validation of the prosthesis on a treadmill using an able-bodied adapter.
- Presents the validation of the device on a treadmill and over level ground tested by a unilateral transfemoral amputee and demonstrates the ability to restore near normal biomechanical gait.

Direction of Future Work

The area of powered lower limbs is a relatively new field of research and offers many unexplored problems that must be addressed to bring such devices to the commercial market. Future areas of research beyond the scope of this dissertation can focus on the three main areas of powered prosthesis design: physical design of the prosthesis, development of prosthesis controllers, and biomechanical evaluations to assess benefits of such a device.

Prosthesis Design

The physical hardware consists of the mechanical and electrical components that comprise the powered prosthesis. A significant requirement of the current design is that in order to generate the requisite torques at the joints requires a transmission ratio on the order of 160:1. At high joint velocities, the ball screws turn at over 10,000 rpm and create an unacceptable audible noise (70 dB at 1 m). The development of a compact and efficient drive mechanism would overcome a significant hurdle and bring a commercially

viable powered prosthesis to the commercial market. A secondary source of audible noise is a high-pitched frequency emitted from the commercial servo amplifiers caused by an inductance mismatch between the servo amplifier and the motor. To alleviate this issue, a useful area of research is to develop a compact servo amplifier better matched to the state-of-the-art brushless DC motors tuned for quiet operation. A custom device could bring further improvements in terms of weight and geometric envelope by allowing the amplifier to be incorporated into the structure for heat sinking. To increase the amputee population aided by such a powered prosthesis, modularity of the design should be sought. Development of separate powered knee and ankle devices that could work both together and independently could better serve the needs of the transfemoral and transtibal amputee communities.

Controller Design

To cover the basic set of functionality provided by a powered lower limb, the finite-state impedance control structures for stair ascent and decent, slope descent, cadence estimation, slope estimation, and uneven terrain compensation need to be developed along with the corresponding supervisory control structure. One drawback of the current finite-state control approach is the considerable amount of manual parameter tuning. To address this issue, an automated, adaptive scheme should to be developed to bring such a powered prosthesis to commercial market. To further increase the efficiency of the tuning process, a more quantitative means to address the performance of the sound-side limb and whole body mechanics to provide a more optimal set of impedance parameters. One potential embodiment of tuning would use a set of accelerometers worn on the body during tuning on the sound side shank and thigh and on the body trunk during tuning. Another interesting focus for future research to the development of alternative control

approach methodologies. One such approach is active-passive control. This method maps the entire state-space of gait to continuous functions rather than a discrete set as in finite-state impedance control. The approach maps passive impedance functions of the knee and ankle joints and supplements the torque output with an active component based on sensor input that measures the user's interaction with the leg, such as the socket sagittal moment sensor. A further area is development of fault detection algorithms to ensure the proper functioning of the device and prevent user injury.

Biomechanical Assessment

A near term study is planned to assess the biomechanics of the amputee subject used in Manuscripts 2 and 3 and Chapter V to study the effects of the powered knee and ankle prosthesis on amputee gait. The measures to be studied would be gait symmetry at three walking speeds (self-selected speed and ±15% of the self-selected speed) in terms of joint angles, moments, powers and stride length and gait posture determined by the motion of the trunk. In addition, metabolic measures such as oxygen intake and heart rate should be considered at the user's self-selected speed to determine if a powered lower limb is capable of reducing the energy expenditure of the user in level ground gait.

Long term future research areas include assessment of the benefits and effects of a powered knee and ankle prostheses on gait and general mobility. These would include standing, transitions between sitting and standing, ascending and descending stairs and ramps, and navigating uneven terrain. Once the physical hardware has achieved a level development where users wear the device as their daily-use prosthesis, a larger study should be conducted. The study, consisting of 10 or more subjects over the course of multiple weeks, would train and accustom users to the device to assess its affect on gait quality

and metabolic energy consumption. In the general study of powered prosthesis, a four quadrant study should be conducted studying the effects of combining active and passive prosthesis and the knee and ankle. This assessment would identify benefits of power at the knee and the ankle joints and help focus future research.